Australian Government

Department of Defence

Defence Science and
Technology Organisation

Signal Processing
in a Semi-active Seeker

Luke Rosenberg, Yiding Hu
and Bill Moran
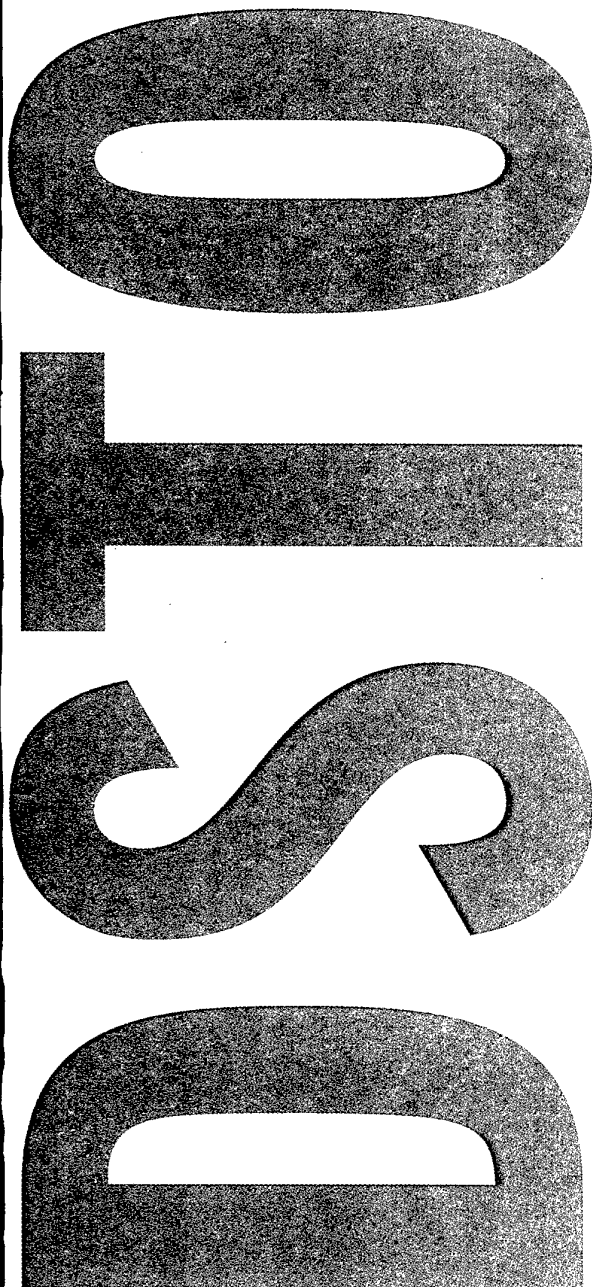
DSTO-TR-1606

20041110 069

Australian Government

Department of Defence

Defence Science and
Technology Organisation

Signal Processing in a Semi-active Seeker

Luke Rosenberg, Yiding Hu

Weapons Systems Division
Systems Sciences Laboratory

Bill Moran

Department of Electrical and Electronic Engineering,
Melbourne University

DSTO–TR–1606

ABSTRACT

In publicly available generic digital simulations of semi-active Radio Frequency (RF) seekers, the combined effect of multipath, sea-clutter and other non-linear noise sources are mainly studied in individual models, while the effect in the seekers data processing has not been systematically investigated. This report details these effects and how they have been combined to model the signal processing blocks inside a semi-active seeker. A basic doppler detection scheme is then simulated to investigate the consequence of these effects on target detection.

RELEASE LIMITATION

AQ F05-01-0144

Conditions of Release and Disposal

This document is the property of the Australian Government. The information it contains is released for defence purposes only and must not be disseminated beyond the stated distribution without prior approval.

The document and the information it contains must be handled in accordance with security regulations applying in the country of lodgement, downgrading instructions must be observed, and delimitation is only with the specific approval of the Releasing Authority as given in the Secondary Release Statement.

This information may be subject to privately owned rights.

The officer in possession of this document is responsible for its safe custody. When no longer required the document should be destroyed and the notification sent to: Reports Officer, DSTO Library, Edinburgh, SA.

Signal Processing in a Semi-active Seeker

EXECUTIVE SUMMARY

In a generic semi-active RF seeker in medium or long range missiles, the combined effect of multipath, sea-clutter and other non-linear noise sources may cause detrimental effects on target detection. This report describes models for each of the effects mentioned and how they can be combined into a single model. A simulation of the combined effects is then used in a simple detection scheme, so that any change in target detection can be assessed.

Authors

Luke Rosenberg
Weapons Systems Division

Luke Rosenberg received his BE (Elec.) with Honours from Adelaide University in 1999 and joined the Missile Simulation Group at DSTO in January 2000. During this time he has completed a Masters degree in Signal and Information Processing through Adelaide University and CSSIP. He is presently studying his PhD at Adelaide University, looking into interference suppression for multi-channel Synthetic Aperture Radar.

Yiding Hu
Weapons Systems Division

(B.Sc 1981, M.Sc 1984, Ph.D 1991, all in physics), 1991-1996, Research Associate and Senior Research Associate at Physics Department, University of Newcastle, Australia. Research area was space physics. 1996-1998, worked on exploration geophysics and mining technologies for Rio Tinto R&D Division at Melbourne as Senior Scientist. 1998-1999, Senior Scientist at World Geoscience, Perth, on R&D of airborne geophysical survey and remote sensing. 1999-present, Senior Research Scientist at the Weapons Systems Division of DSTO, working on analysis of weapon systems.

Bill Moran
Dept. of Electrical & Electronic Engineering, Melb. University

Bill Moran has been a Professor of Electrical Engineering at the University of Melbourne since July 2001. Previously was Professor of Mathematics at Flinders University (1991–2001) and at the University of Adelaide (1976–1991). He has a B.Sc. (Hons) degree in Mathematics from the University of Birmingham in the UK and a Ph.D. from the University of Sheffield. He was elected a Fellow of the Australian Academy of Science in 1984. From 1991 to 1998, he was a Program Leader in the Cooperative Research Centre for Sensor Signal and Information Processing. His research areas in mathematics include harmonic analysis, representation theory and number theory. More recently he has added research interest in several aspects of signal processing. He is CEO of Eudoxus Consulting, through which he does much of his current work with DSTO.

Contents

Appendices

Figures

Tables

Glossary

AOA   Angle Of Arrival
AC   Alternating Current
AFC   Automatic Frequency Control
CW   Continuous Wave
DC   Direct Current
IF   Intermediate Frequency
LO   Local Oscillator
LOS   Line Of Sight
MLC   Main Lobe Clutter
PDF   Probability Distributions Function
ROC   Receiver Operating Characteristic
RF   Radio Frequency
SLC   Side Lobe Clutter
VCO   Voltage Controlled Oscillator

1   Introduction

1.1   Project Aim

In a generic semi-active RF seeker in medium or long range missiles, the signals at the front and rear receivers are mixed to shift the carrier frequency to an Intermediate Frequency (IF) where the target's doppler shift can be detected. When the missile is used against low altitude targets in the presence of multipath in the rear receiver and sea-clutter and multipath in the front receiver, the mixing of these two signals will significantly affect the seeker's ability to detect a target correctly.

In publicly available generic digital simulations of semi-active RF seekers, there has been substantial research into both multipath, [1]-[3] and sea-clutter, [4]-[5]. The aim of this project is to combine these effects into a single model, simulate them and investigate the mixing of the front and rear signals. A target detection scheme is then used to determine the effect on target detection.

The report starts by describing a classical model for a Continuous Wave (CW) seeker and a simplified version used for simulation. The second section describes three effects: multipath, sea-clutter and receiver noise, which are used to increase the realism in the model. The final section focusses on doppler detection and outlines an optimal detection scheme as well as a classical non-optimal detector described in Skolnik, [6]. This is extensively modelled and Receiver Operating Characteristics (ROC) are compared for both an ideal simulation and a realistic one using the three effects.

1.2   Problem Description

A typical encounter with a missile containing a semi-active RF seeker against sea-skimming targets is shown in Figure 1. The seeker system has two receivers, one at the front and the other at the rear. As a semi-active system, it contains no active radar and is completely dependent on the launch platform to illuminate the target and provide relevant information about the frequency of the illuminating beam and its modulation, if any.

As the target and the missile approach each other, two doppler shifts arise. The first is from the launch platform to the missile and the second is from the launch platform reflected off the target and incident on the seeker. This differential doppler allows the seeker to identify and lock onto the target by carefully combining and filtering the two incoming signals. To calculate the position of the target, a monopulse receiver at the front of the seeker measures the angle of arrival (AOA) of the target signal in azimuth and elevation. This information will be noisy however, due to multipath reflections, sea-clutter and non-linearities from the hardware in the seeker.
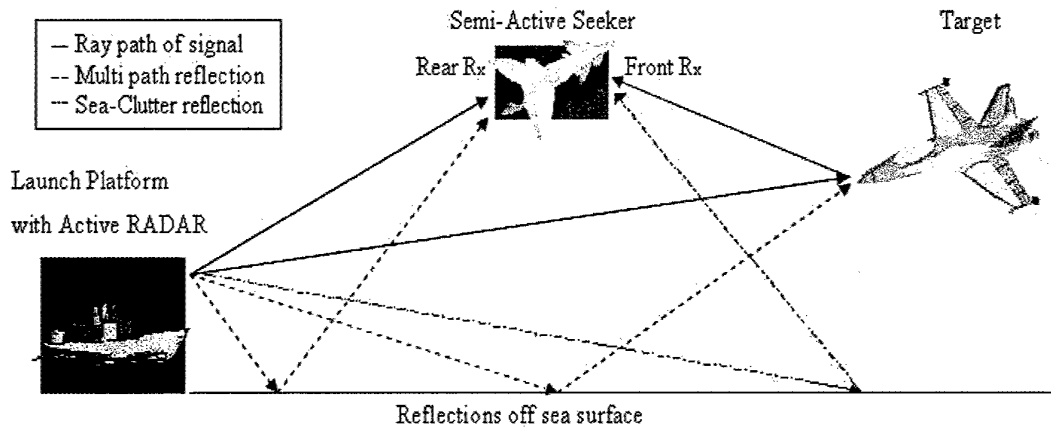
Figure 1: Problem scenario with multipath and sea-clutter reflections

2 The Semi-Active Seeker

2.1 Classic Model

The block diagram in Figure 2, [6], is representative of the earliest systems developed in the late 1940's and early 1950's. It is the simplest representation of a semi-active CW seeker and consists of a rear receiver, a front receiver, a signal processor (speedgate), and a tracking loop to control the gimballed front antenna. The missile also contains an autopilot to guide it and stabilize the airframe, a fuze to detonate the warhead at the optimum time, and a source of electrical and (in most missiles) hydraulic power.
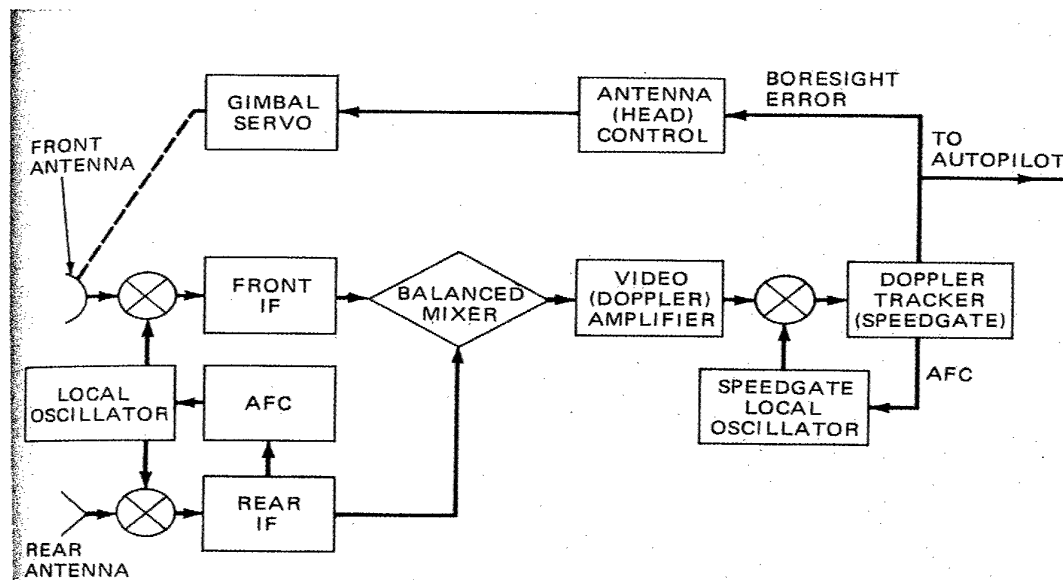
Figure 2: Semi-active seeker block diagram

The purpose of the rear reference receiver is to provide a coherent reference for the detection of the front or target signal. The rear signal, after conversion to IF, closes the Automatic Frequency Control (AFC) loop around the microwave Local Oscillator (LO) and acts as the reference for the IF coherent detector. The target signal, received at the front antenna, is heterodyned to IF and amplified in a relatively wideband amplifier. It is then converted to the baseband by mixing with the rear signal in the balanced mixer.

The doppler signal, now at baseband, is amplified in the video (doppler) amplifier, which has a bandwidth equal to the total range of possible doppler frequencies. It is then mixed with the speedgate LO, which is controlled by an AFC loop to keep the desired signal centered in the narrow speedgate (sometimes called the velocity gate or doppler tracker). Target detection is covered more thoroughly in section 4.

2.2 Simplified Model

The semi-active seeker model detailed in the previous section is now simplified so the effect of different noise sources in the doppler output can be studied.

- The AFC has been removed as both front and rear signals are created from ideal frequency sources.

- The gimbal servo and antenna control has been removed, as the front receiver is assumed to point to the target and the rear receiver is fixed at the exit direction with a broad view angle.

- The first mixing stage including the LO has also been removed, as simulating an RF signal in the Gigahertz band is not feasible. Also, the effect of amplifying the IF signals in the Front and Rear IF blocks may not have a big effect on the final doppler measurement. A low pass filter has been included in its place and is placed after the mixer to remove unwanted high frequency signals.

- The section after the balanced mixer is addressed separately in section 4.

The resulting model is shown in Figure 3.

The mixing of the front and rear signals, S_R and S_F is either a multiplication in the time domain, or a convolution in the frequency domain.

In the time domain:
$$S_D(t) = S_R(t)S_F(t) \tag{1}$$

In the frequency domain:
$$S_D(f) = S_R(f) \otimes S_F(f) \tag{2}$$

The low pass filter is then used to remove unwanted high frequency components (see section 2.3).

3
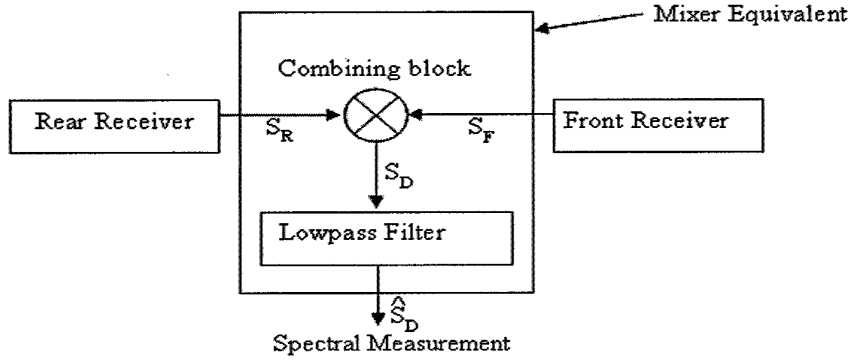
Figure 3: Simplified semi-active seeker signal processing block diagram

2.3 Doppler

The doppler effect is a shift in the frequency of a wave radiated, reflected or received by an object in motion. In the scenario for this project, a stationary illuminator is tracking a moving target and the radio waves either compress or stretch when they come in contact with the target. The doppler frequency equals the rate of change of the distance to the target d, divided by the wavelength.

$$f_d = -\frac{\dot{d}}{\lambda} \tag{3}$$

The minus sign accounts for the fact that, if $\dot{d}$ is negative (closing target), the doppler frequency is positive.

The seeker makes use of the differential doppler frequency to distinguish small but fast moving airborne targets from each other and from any background terrain and clutter. Early doppler homers used pure CW illumination of the target, but recently the tendency has been to employ some type of modulation such as pulse or CW frequency modulation. A system with a modulation scheme is able to determine both range and range rate simultaneously, but for simplicity the simulation in this project is a pure CW system. The geometry for an ideal doppler shift of the front and rear receivers is shown in Figure 4, [7].

Let the illuminator (I) carrier frequency be f_c, the missile and target velocities, u_m and u_t respectively. The target (T) receives a frequency $f_c + \left(\frac{u_t}{\lambda}\right) \cos\beta$ due to a movement of T with respect to I. This then re-radiates towards the missile (M) with a further doppler shift of $\left(\frac{u_t}{\lambda}\right) \cos\alpha$ due to M travelling towards T. The missile is also affected by that motion and has a doppler shift of $\left(\frac{u_m}{\lambda}\right) \cos\delta$. Hence the front receiver on the seeker receives a signal with frequency

$$f_c + \frac{u_m \cos\delta + u_t(\cos\alpha + \cos\beta)}{\lambda}. \tag{4}$$

The mixer inside the seeker extracts the target's doppler, f_D, by comparing this frequency with that of the rear reference, which is

$$f_c - \frac{u_m \cos\gamma}{\lambda} \tag{5}$$
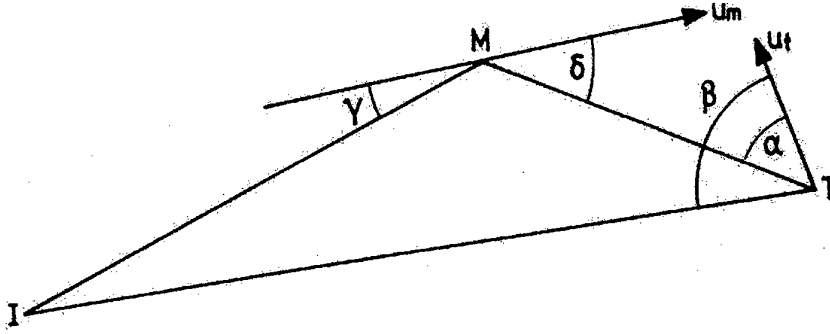
Figure 4: Semi-active homing target geometry

due to a movement of M away from I. Now, define

$$f_F = \frac{u_m \cos \delta + u_t (\cos \alpha + \cos \beta)}{\lambda}$$

$$f_R = -\frac{u_m \cos \gamma}{\lambda}$$

and when two CW signals at these frequencies are multiplied in the time domain as in equation 1, the following occurs:

$$\begin{aligned} S_D(t) &= A_F \sin(2\pi(f_c + f_F)t) A_R \sin(2\pi(f_c + f_R)t) \\ &= \frac{A_F A_R}{2} \left[\cos(2\pi(f_F - f_R)t) - \cos(2\pi(2f_c + f_F + f_R)t) \right] \end{aligned} \tag{6}$$

where each signal has zero phase. After low-pass filtering the result, and sampling high enough to see only the bottom part of the spectrum where the final doppler will be, the final amplitude of the doppler signal, $\hat{S_D}$ is:

$$A_D = \frac{A_F A_R}{2} \tag{7}$$

with corresponding doppler frequency:

$$\begin{aligned} f_D &= f_F - f_R \\ &= \frac{u_m(\cos \delta) + u_t(\cos \alpha + \cos \beta)}{\lambda} + \frac{u_m \cos \gamma}{\lambda} \\ &= \frac{u_m(\cos \delta + \cos \gamma) + u_t(\cos \alpha + \cos \beta)}{\lambda}. \end{aligned} \tag{8}$$

The maximum value of f_D occurs when I, M and T are collinear and M and T are flying towards each other, giving

$$f_{D_{max}} = \frac{2(u_m + u_t)}{\lambda}. \tag{9}$$

3 Simulated Effects

Equation 8 represents ideal line spectra. However, in real life the spectra spreads in frequency, making computation more complicated. Effects such as main lobe sea-clutter which will cause an extra peak, multipath reflections which spread the front and rear signals and receiver noise will alter the ideal spectrum. To explore these effects, simulation is required.

The simulation for this section was written in MATLAB, using Simulink for the simulation and signal processing. The CW or carrier frequency is chosen as 10GHz which corresponds to an X-band radar. However, the concerned positive and negative doppler effects will be around 10GHz. Therefore, the CW frequency was used as a reference and a sampling rate cover range of 4MHz was used to give a spectra range of 10GHz±2MHz.

The simulation is done entirely in the frequency domain to simplify the addition of the external effects. Consequently, the mixing is now a convolution instead of a multiplication in the time domain. The effect of convolving two signals is a lengthening of the vector, a final amplitude dependent on the length of the input and triangulation. For example, if two uniform signals X_1 and X_2 have lengths N and M respectively, then $X_1 \otimes X_2$ has length $M + N - 1$ and the spectrum is shown in Figure 5.
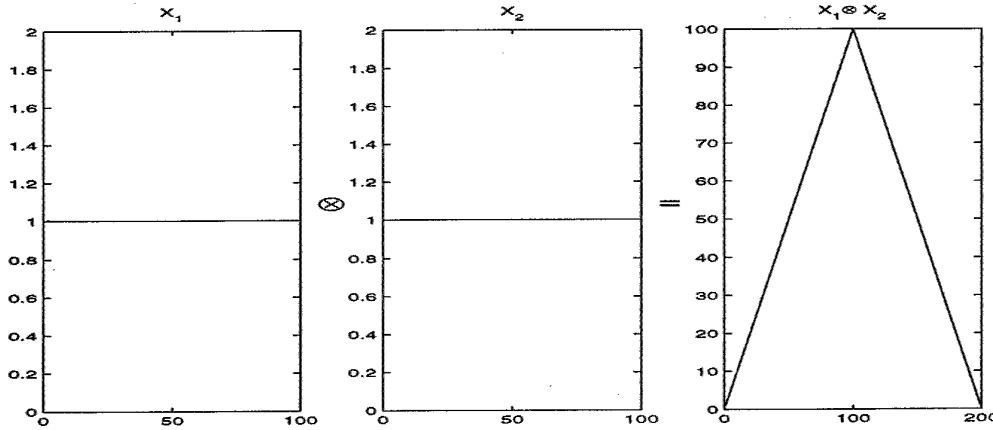
Figure 5: Convolution example

The CW signal at the illuminator is modelled as a Gaussian shape with a small frequency spread σ^2_{CW} and a mean frequency, μ_{CW} equal to 10GHz.

$$S_{CW}(f) = \frac{1}{\sqrt{2\pi\sigma^2_{CW}}} \exp\left[-\frac{(f - \mu_{CW})^2}{2\sigma^2_{CW}}\right] \tag{10}$$

The front and rear CW signals are then created in the simulation by adding a further doppler shift specified by the parameters in the scenario. The frequency offsets for the front and rear signals are defined as μ_1 and μ_2.

To increase realism, three noise sources have been included before mixing, (1) multipath in the front receiver, (2) main-lobe sea-clutter in the front receiver and (3) receiver noise in both the front and rear receivers. The simulation runs for a single time period, so the missile and the target are at a constant velocity and do not change their position. Two test scenarios were created for the analysis and have the following parameters:

Table 1: Scenario parameters

Scenario no.	α (°)	β (°)	δ (°)	γ (°)	Missile velocity, u_m (m/s)	Target velocity, u_t (m/s)	Doppler - front (kHz)	Doppler - rear (kHz)
1	0	0	0	0	900	300	50	-30
2	60	90	60	60	900	300	20	-15

The first set of parameters was chosen as an ideal case where the target, missile and illuminator are in a straight line. The missile velocity is set to three times the target velocity and the target is assumed to be incoming. The second set of parameters are a little more realistic and have the target flying straight up trying to avoid the incoming missile.

3.1 Ideal Simulation

The ideal simulation results, without any extra effects, are shown in Figures 6 and 7. They are based on equation 11, which is represented in the frequency domain.

$$\mathbf{S_D} = \mathbf{S_R} \otimes \mathbf{S_F} \tag{11}$$

For both scenarios, the results clearly show the target's doppler at 80kHz and 35kHz respectively. A verification for this simulation is given in Appendix A.
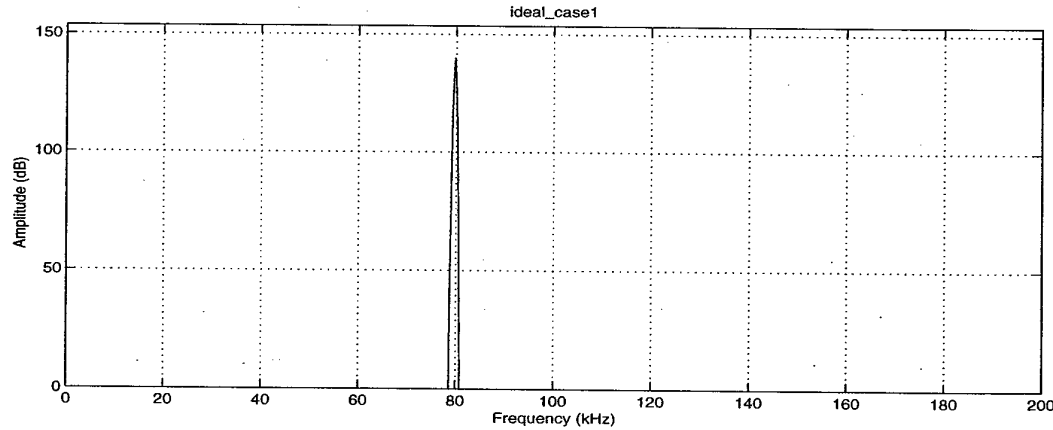
Figure 6: Ideal scenario 1
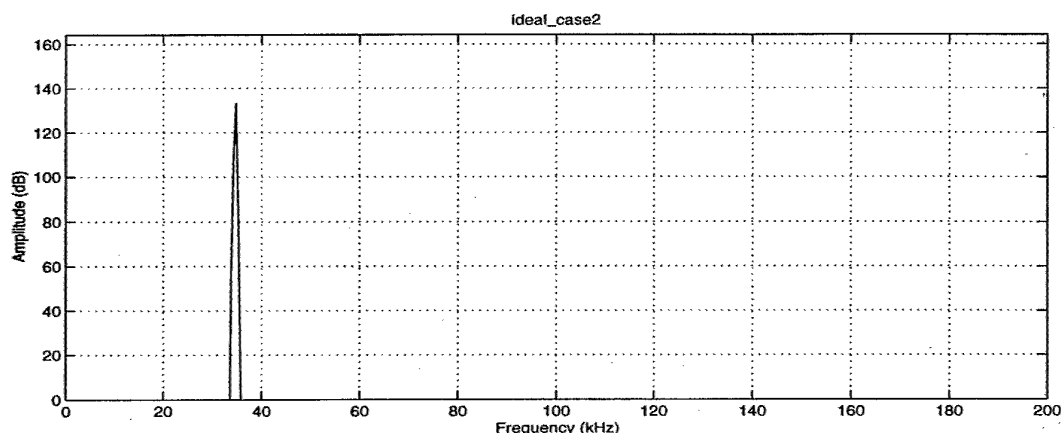
Figure 7: Ideal scenario 2

3.2 Multipath Reflections

Multipath effects come about by reflections on the surface of the sea and by ducting, [2]. Multipath reflections from the sea can be either specular or diffuse. The specular component is coherent with respect to the direct signal, and is well defined in terms of amplitude, phase and incident direction. The diffuse component has a random nature, and arises from scattering sources from many directions. These paths are shown in Figure 8, [3].
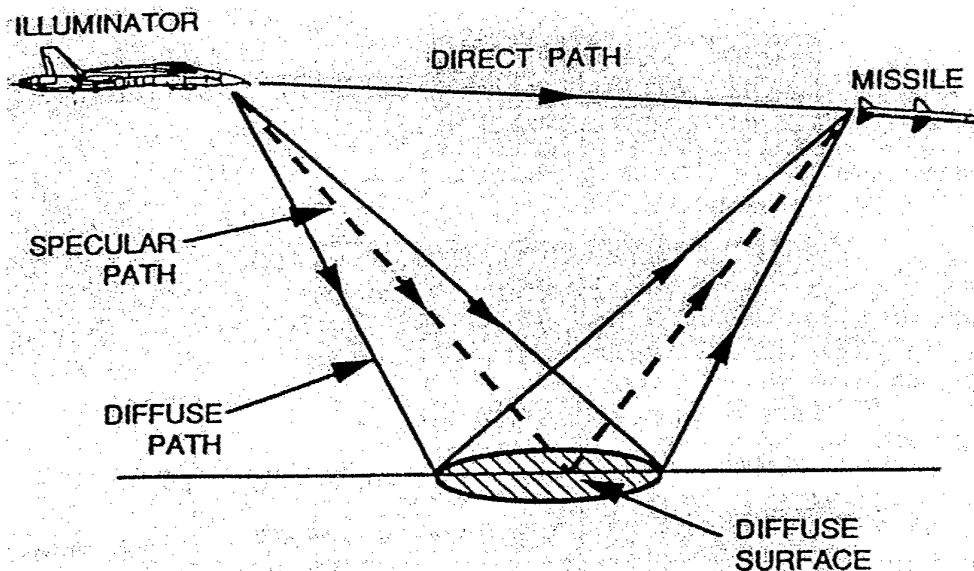
Figure 8: Rear multipath components

A duct is a layer of air with different properties than its surroundings and acts as a waveguide to trap electromagnetic energy. These refractive gradients in the atmosphere can cause over-the-horizon fields to be tens of decibels higher than expected. More detail

about ducting can be found in [2] and [6]. For this project, only the effect of optical interference has been included.

Due to the small grazing angle in the scenario for this project, multipath reflections are likely to be strong, even with high sea states. According to plane earth reflection theory, the one-way voltage reflection factor is $2\sin(\frac{2\pi h_1 h_2}{\lambda R})$, where h_1 and h_2 are the radar and target heights respectively and R is the range. Practical values and a more comprehensive explanation are given by James in [7].

In the semi-active scenario, there are three ways for multipath forward scattering: (1) the transmit path from illuminator to missile rear receiver, (2) the transmit path from the illuminator to target, and (3) the receive path from the target to missile in the front receiver (see Figure 9, [3]). In this simulation, we consider only multipath corruption of the rear signal.
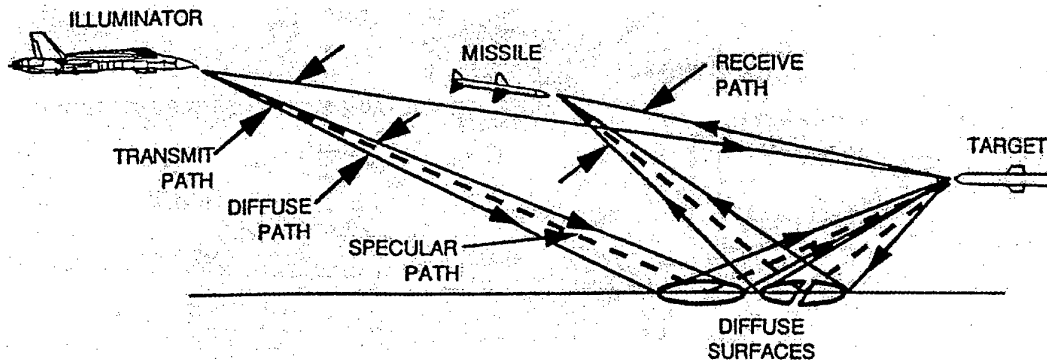
Figure 9: Front multipath components

It has been shown, [1] that the effect of multipath reflections distorts the final doppler signal by widening the spectrum. For the simulation in this project, the rear signal, S_R will change from a line spectrum to a broad spectrum, where the spread in rear signal accounts for both the specular and diffuse paths.

Multipath in the front receiver was studied as a special case of the multiple target problem, where resolving two closely spaced targets is very difficult. In tracking radar, the presence of unresolved targets will degrade the quality of the data obtained. In a guidance system, the approach used to overcome this is to minimize the reflected (image) signal and also prevent the 'noise' in the pitch (elevation) plane guidance channel from causing the missile to impact the surface during low-altitude intercepts. In the case of the sea-skimming anti-ship missile, this is done by implementing a radar altimeter for guidance in the elevation plane, and by only using the target angle data in azimuth.

3.2.1 Simulation Results

There are many models that can be used to simulate the multipath signal. The multipath signal for this project is created by the original CW signal with no doppler shift,

S_{CW}, convolved with a multipath function, M. M is a Gaussian centered at the rear doppler and the result of this convolution is another Gaussian centered with a frequency shift μ_2, the same as the rear signal. The resultant is modelled with amplitude A_M and a very broad user specified frequency spread σ_M^2. In reality, the spectrum would skew to the left as the doppler shift in the diffuse path is smaller.

$$
\begin{aligned}
S_M(f) &= S_{CW}(f) \otimes M(f) \\
&= \frac{A_M}{\sqrt{2\pi\sigma_M^2}} \exp\left[-\frac{(f-\mu_2)^2}{2\sigma_M^2}\right]
\end{aligned}
\tag{12}
$$

The rear signal can then be represented as the sum of direct and diffuse components:

$$
\mathbf{S_R'} = \mathbf{S_R} + \mathbf{S_M}
\tag{13}
$$

The spread rear signal is then further spread by the convolution and the equation for the doppler output signal can now be updated:

$$
\mathbf{S_D} = (\mathbf{S_R} + \mathbf{S_M}) \otimes \mathbf{S_F}
\tag{14}
$$

Figures 10 and 11 demonstrate the multipath reflections for each scenario.
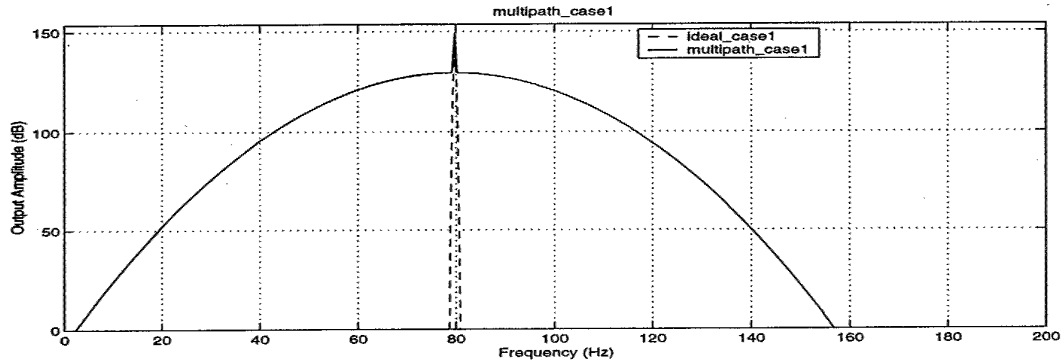

Figure 10: Scenario 1 with multipath reflections
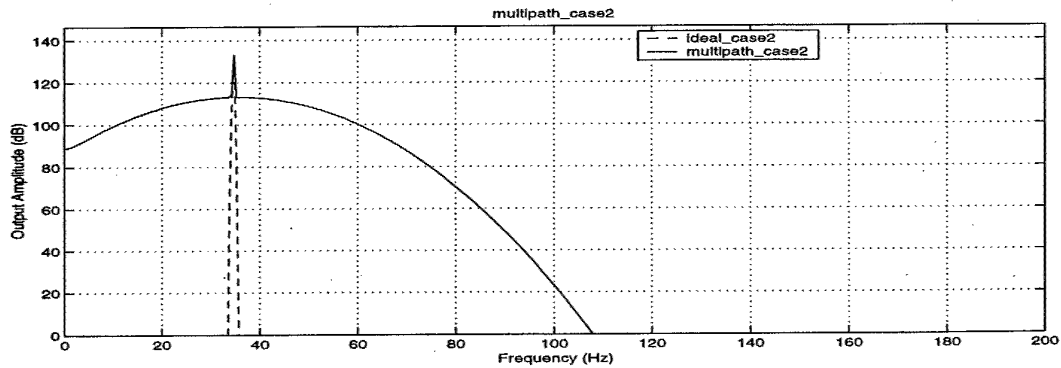
Figure 11: Scenario 2 with multipath reflections

In each of the above figures, it is clear that the original signal is greatly spread in frequency. This amount of spread was chosen to give a better comparison to real life.

3.3　Sea Clutter

As the sea-skimming target is being illuminated, there is a large amount of background clutter. This sea clutter is then seen by the front receiver on the missile which is looking down at the target (see Figure 12).
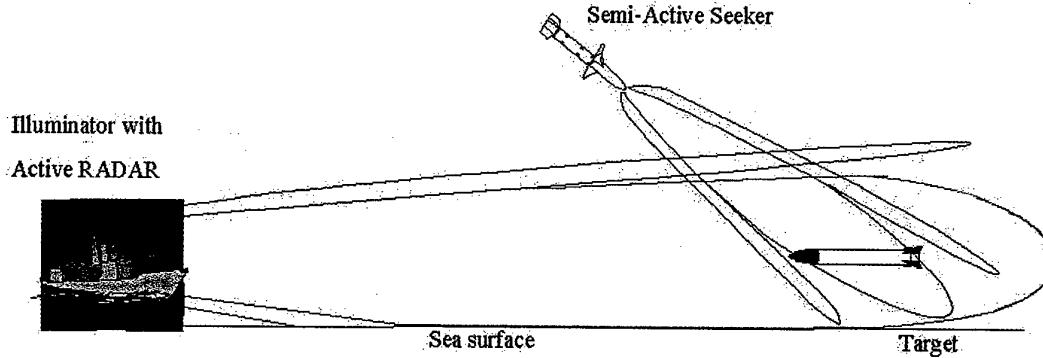
Figure 12: Front and side-lobe clutter for a sea-skimming missile

The return from the sea is made up of two main parts, main-lobe and side-lobe return and is typically different for different sea states and atmospheric conditions. In general, the power of the return from a small patch of ground, at a given transmitter frequency is given by

$$P_r \propto \frac{P_{avg}G^2\sigma A_g}{R^4} \tag{15}$$

where

$$
\begin{aligned}
P_{avg} &= \text{average transmitted power} \\
G &= \text{gain of radar antenna in the direction of the patch } (G^2 = \text{two way gain}) \\
\sigma &= \text{factor called the incremental backscattering coefficient} \\
A_g &= \text{resolvable area of ground (ground patch)} \\
R &= \text{range of ground patch}
\end{aligned}
$$

The backscattering coefficient, σ is the radar cross section of a small increment of ground area, ΔA. This parameter is explained further in [8].

3.3.1　Main-lobe return

Main-lobe return or Main-lobe Clutter (MLC) is produced whenever the main-lobe intercepts the sea. Because the area intercepted by the main-lobe can be extensive and the gain of the main-lobe is high, main-lobe return is generally quite strong.

The spectral characteristics of main-lobe return are best understood by visualizing the ground area illuminated by the main-lobe as consisting of a large number of small

individual patches. The doppler frequency of each patch, f_{cl} is proportional to the cosine of the angle α, between the missile velocity and the Line of Sight (LOS) to the patch.

$$f_{cl} = \frac{u_m \cos \alpha}{\lambda} \tag{16}$$

where

$$\begin{aligned} u_m &= \text{velocity of missile} \\ \alpha &= \text{angle between the missile and LOS to the ground patch} \\ \lambda &= \text{wavelength} \end{aligned}$$

The angle α is not the same for every part of the patch. As a result, the collective return occupies a band of frequencies.

For the case when the antenna is looking straight ahead, the doppler frequency of the return from the patches near the center of the illuminated area very nearly equals its maximum possible value:

$$f_{cl_{max}} = \frac{u_m}{\lambda}. \tag{17}$$

3.3.2 Side-lobe return

The clutter signal received from the antenna side-lobes, also called Side Lobe Clutter (SLC) is always undesirable. It tends to be less concentrated (less power per unit of doppler frequency) than the main-lobe clutter, but covers a much wider band of frequencies. Side-lobes extend in virtually all directions, therefore regardless of the antenna look angle, there are always side-lobes pointing ahead, behind and every angle in between. The band of frequencies covered by the side-lobe clutter extends from a positive frequency, corresponding to the radar velocity ($f_d = \frac{u_m}{\lambda}$), to an equally negative frequency. The extent to which side-lobe clutter is a problem, depends on many things:

- Frequency resolution provided by the radar

- Range resolution provided by the radar

- Gain of the side-lobes

- Altitude of the radar

- Backscattering coefficient and angle of incidence

- Man-made objects in the terrain

3.3.3 Simulation Results

In the simulation, only MLC has been included, as the effect of SLC on doppler is negligible compared to a peak that is near or overlapping a target signal. The sea-clutter

signal is created in the frequency domain with a Gaussian shape, user defined amplitude A_C, broad frequency spread σ_{cl}^2 and frequency offset f_{cl}.

$$S_C(f) = \frac{A_C}{\sqrt{2\pi\sigma_{cl}^2}} \exp\left[-\frac{(f - f_{cl})^2}{2\sigma_{cl}^2}\right] \tag{18}$$

This distribution is not an exact representation of real life, as there are many parameters involved which shape the MLC. It was chosen as a simple model to use in this simulation and could be improved in future work. In the simulation, the sea-clutter signal is added to the front signal, which now becomes:

$$\mathbf{S_F'} = \mathbf{S_F} + \mathbf{S_C} \tag{19}$$

where $\mathbf{S_F}$ is the original front signal. The equation for the doppler output signal can now be updated:

$$\mathbf{S_D} = \mathbf{S_R} \otimes (\mathbf{S_F} + \mathbf{S_C}) \tag{20}$$

where the effect of the convolution is to further spread the sea-clutter signal. For the scenarios in this project, the desired frequency offset, f_{cl} is set to the corresponding doppler between the missile and the ground offset by 20° to represent the peak sea-clutter signal not being directly at the line of sight.

$$f_{cl} = \frac{u_m \cos(20°)}{\lambda} \tag{21}$$

For both scenarios, the missile's velocity u_m is 300m/s, and equation 21 gives a frequency of 28.21kHz. The mixing then causes the center frequency to shift to the right by subtracting the rear doppler component. Hence, the expected frequency for scenario 1 is 28.21kHz − (−30kHz) = 58.21kHz and 28.21kHz − (−15kHz) = 43.21kHz for scenario 2. This calculation is detailed in Appendix B.

Figures 13 and 14 show the results from the Simulink model. The amplitude of the sea-clutter signal is set to be slightly lower than the target signal, and the spread is large to give a better comparison to real life. In each case, it is clear that the added signal is at the correct frequency and the characteristic of the sea-clutter signals are correct.
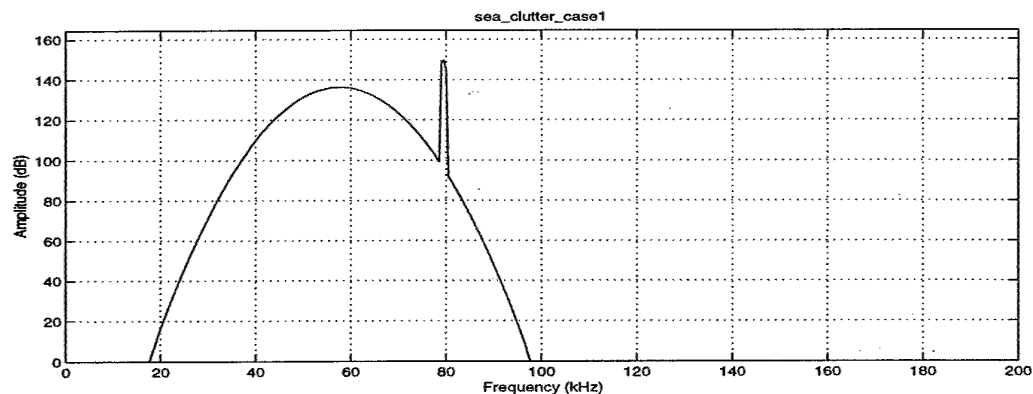
Figure 13: Scenario 1 with sea-clutter
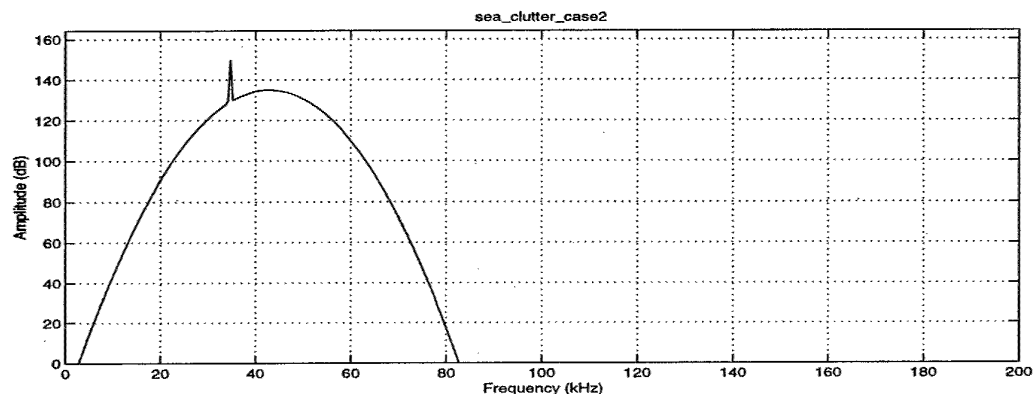
Figure 14: Scenario 2 with sea-clutter

3.4   Receiver Noise

3.4.1   Noise Fundamentals

Receivers generate thermal noise which masks weak echoes being received from the radar transmissions. This noise is one of the fundamental limitations on the radar range and is shown in the range equation for a bi-static radar, where the transmitter and receiver are separated (see Appendix D).

Most of this noise originates in the input stages of the receiver. The reason is not that these stages are inherently more noisy than others but when amplified by the receiver's full gain, noise generated there swamps out the noise generated further along. Since the noise and the received signals are thus amplified equally, in computing signal-to-noise ratios, the factor of receiver gain can be eliminated by determining the signal strength at the input to the receiver and dividing the noise output of the receiver by the receiver gain. Thus, the receiver noise is commonly defined as noise per unit of receiver gain.

$$\text{Receiver noise} = \frac{\text{Noise at output of receiver}}{\text{Receiver Gain}} \tag{22}$$

More commonly, the noise performance Figure of merit is known as the 'noise figure', F_n. This is the ratio of the noise output of the actual receiver to the noise output of a hypothetical, 'ideal' minimum-noise receiver providing equal gain.

$$F_n = \frac{\text{Noise output of actual receiver}}{\text{Noise output of ideal receiver}} \qquad (23)$$

Thermal noise is spread more or less uniformly across the entire spectrum, [8]. So, the amount of noise appearing in the output of the ideal receiver is proportional to receiver bandwidth. The mean power per unit of receiver gain, of the noise in the output of the the hypothetical ideal receiver is thus:

$$\text{Mean noise power (ideal receiver)} = kT_0B \ (W) \qquad (24)$$

where B is the receiver bandwidth and by convention, T_0 is taken to be $290°K$, which is close to room temperature and makes kT_0 a round number (4×10^{-21} Ws).

When the internally generated noise is considerably greater than the external noise, the noise figure, F_n, multiplied by the previous expression for mean noise power per unit of gain for an ideal receiver is commonly used to represent the level of background noise against which target echoes must be detected.

$$\text{Mean noise power (actual receiver)} = F_n k T_0 B \ (W) \qquad (25)$$

Typically though, the noise temperature of the radar receiver is not the most important characteristic, since choosing a low noise amplifier will sacrifice other important performance characteristics such as dynamic range, instantaneous bandwidth, phase amplitude stability and cooling in the receiver.

3.4.2 Noise Statistics

It is important that the noise modelled in this section accurately produces the correct statistics, otherwise the target detection schemes in section 4 will not work properly. To this end, the following hypothesis for the output signal is defined and a derivation of the Probability Distribution Functions (PDF) for each case follows:

$$H_0: \qquad \text{noise only is present} \rightarrow n(t)$$
$$H_1: \qquad \text{signal and noise are present} \rightarrow s(t) + n(t)$$

The additive zero mean white noise $n(t)$, is spatially incoherent and uncorrelated with variance σ^2. It is added to both magnitude and phase and hence has a complex representation.

Consequently, the front and rear signals can be written as a combination of real (in-phase) and imaginary (quadrature) parts, separated by a phase of $90°$.

$$
\begin{aligned}
\nu(t) &= \nu_I(t)\cos(2\pi f_{in}t) + \nu_Q(t)\sin(2\pi f_{in}t) \\
&= r(t)\cos(2\pi f_{in}t - \phi(t))
\end{aligned}
$$

or simply

$$
\begin{aligned}
\nu_I(t) &= r(t)\cos(\phi(t)) \\
\nu_Q(t) &= r(t)\sin(\phi(t))
\end{aligned}
$$

where $f_{in} = f_c + f_R$ and $f_c + f_F$ for the rear and front signals respectively, $r(t)$ is the amplitude of $\nu(t)$ and the phase, $\phi(t) = \arctan(\frac{\nu_Q}{\nu_I})$.

If we run a test scenario where there is no target, then the in-phase and quadrature components are:

$$
\begin{aligned}
\nu_I(t) &= n_I(t) \\
\nu_Q(t) &= n_Q(t)
\end{aligned}
$$

and likewise, if we know there is a target present with an amplitude A:

$$
\begin{aligned}
\nu_I(t) &= A + n_I(t) \Rightarrow n_I(t) = r(t)\cos(\phi(t)) - A \\
\nu_Q(t) &= n_Q(t) = r(t)\sin(\phi(t)).
\end{aligned}
$$

where the noise in-phase and quadrature components $n_I(t)$ and $n_Q(t)$ are uncorrelated zero mean Gaussian with equal variances σ^2. The joint PDF of the two random variables $n_I; n_Q$ is

$$
\begin{aligned}
f(n_I; n_Q) &= \frac{1}{2\pi\sigma^2}\exp\left(-\frac{n_I^2 + n_Q^2}{2\sigma^2}\right) \\
&= \frac{1}{2\pi\sigma^2}\exp\left(-\frac{(r\cos\phi - A)^2 + (r\sin\phi)^2}{2\sigma^2}\right)
\end{aligned}
\tag{26}
$$

Now, the PDF's of the random variables $r(t)$ and $\phi(t)$, represent the modulus and phase of $\nu(t)$. The joint PDF of these two random variables $r(t); \phi(t)$ is given by

$$
f(r; \phi) = f(n_I; n_Q)|J|
\tag{27}
$$

where the Jacobian is:

$$
J = \begin{bmatrix} \frac{\partial n_I}{\partial r} & \frac{\partial n_I}{\partial \phi} \\ \frac{\partial n_Q}{\partial r} & \frac{\partial n_Q}{\partial \phi} \end{bmatrix} = \begin{bmatrix} \cos\phi & -r\sin\phi \\ \sin\phi & r\cos\phi \end{bmatrix}
$$

with determinant $|J| = r$. Substituting this result and equation 26 into equation 27 gives:

$$
\begin{aligned}
f(r; \phi) &= \frac{r}{2\pi\sigma^2}\exp\left(-\frac{(r\cos\phi - A)^2 + (r\sin\phi)^2}{2\sigma^2}\right) \\
&= \frac{r}{2\pi\sigma^2}\exp\left(-\frac{r^2 + A^2}{2\sigma^2}\right)\exp\left(-\frac{rA\cos\phi}{\sigma^2}\right)
\end{aligned}
\tag{28}
$$

Then to obtain the PDF for r alone, we need to integrate over ϕ.

$$
\begin{aligned}
f(r) &= \int_0^{2\pi} f(r; \phi)d\phi \\
&= \frac{r}{\sigma^2}\exp\left(-\frac{r^2 + A^2}{2\sigma^2}\right)\frac{1}{2\pi}\int_0^{2\pi}\exp\left(-\frac{(rA\cos\phi)}{\sigma^2}\right)d\phi
\end{aligned}
\tag{29}
$$

where the integral inside equation 29 is known as the modified Bessel function of order zero:

$$
I_0(\beta) = \frac{1}{2\pi}\int_0^{2\pi} e^{\beta\cos\theta}d\theta
\tag{30}
$$

Thus,

$$f(r) = \frac{r}{\sigma^2} I_0 \left(\frac{rA}{\sigma^2} \right) \exp \left(-\frac{r^2 + A^2}{2\sigma^2} \right) \qquad (31)$$

which is the Rice PDF. If the scenario contains noise only, then $\frac{A}{\sigma^2} = 0$ and equation 31 becomes a Rayleigh PDF:

$$f(r) = \frac{r}{\sigma^2} \exp \left(-\frac{r^2}{2\sigma^2} \right) \qquad (32)$$

and if there is a target with the noise, then $\frac{A}{\sigma^2}$ is very large and equation 31 becomes a Gaussian PDF, with mean A and variance σ^2:

$$f(r) = \frac{1}{\sqrt{2\pi\sigma^2}} \exp \left(-\frac{(r-A)^2}{2\sigma^2} \right) \qquad (33)$$

The PDF for the random variable ϕ is found likewise, but not described here. If we look at the noise statistics of the simulation over 200 runs, the amplitude distributions of target with noise and noise alone match the theoretical distributions. One is a Gaussian, while the other is a Rayleigh distribution.
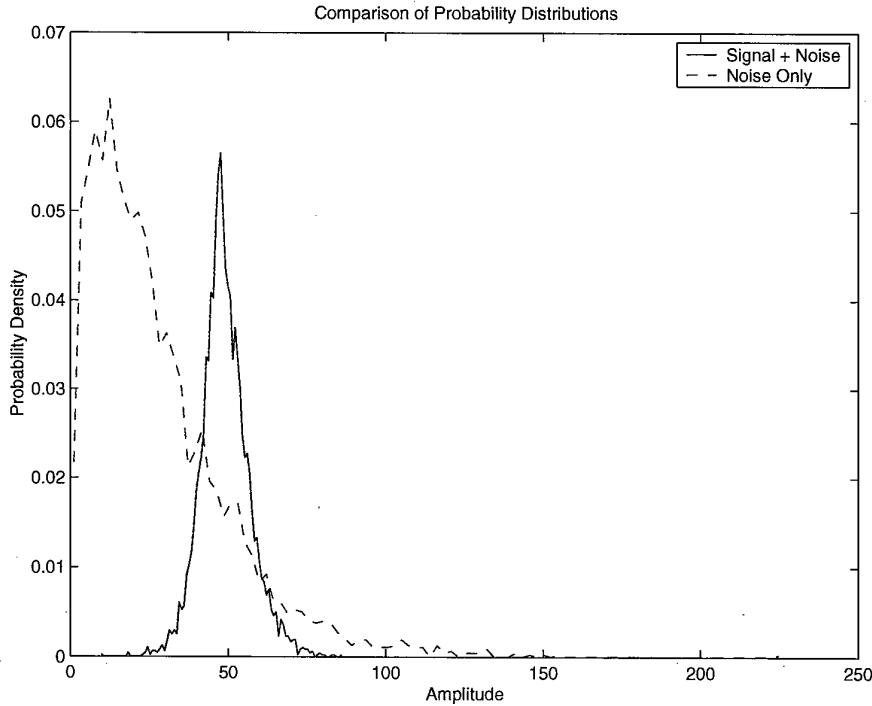
Figure 15: Simulation probability distributions

3.4.3 Simulation Results

In the simulation, the receiver noise **N**, used is additive zero-mean coloured noise with an amplitude determined by the user defined noise power level. This signal is added to both the front and rear receiver blocks in the Simulink simulation. The equation for the doppler output signal can now be updated:

$$\mathbf{S_D} = (\mathbf{S_R} + \mathbf{N}) \otimes (\mathbf{S_F} + \mathbf{N}) \tag{34}$$

Scenario's 1 and 2 are shown in figures 16 and 17. They both clearly show the effect of the randomness over the entire spectrum.
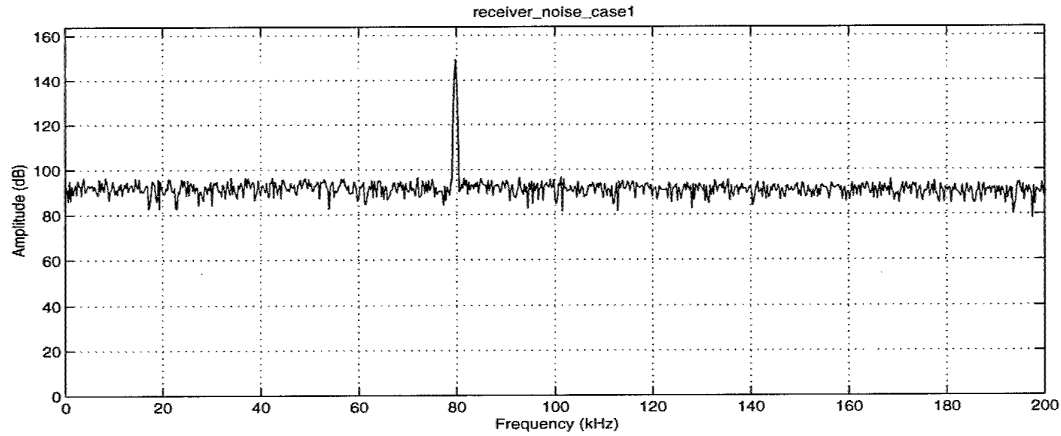
Figure 16: Scenario 1 with receiver noise
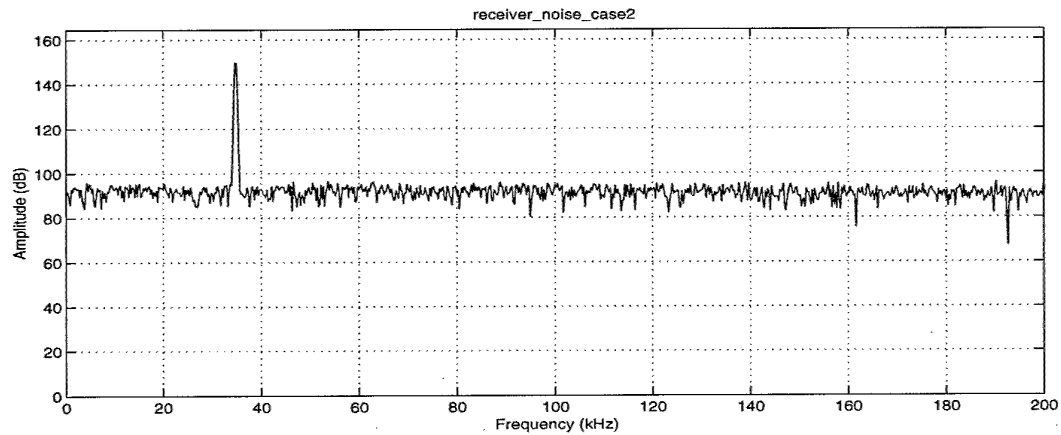
Figure 17: Scenario 2 with receiver noise

3.5 Complete Simulation

The last stage of the simulation is to combine the three effects together. The final equation for the doppler output is:

$$S_D = (S_R + S_M + N) \otimes (S_F + S_C + N) \tag{35}$$

where the different amplitudes are determined by the user. Simulation results are shown in figures 18 and 19. The spectra's clearly show the sea-clutter peak at the correct frequency, the spread target signal and random noise over the entire spectrum. When the combination of the sea-clutter and multipath merge together, only the tip of the target is clear.

Figure 18: Scenario 1 with all three effects combined

Figure 19: Scenario 2 with all three effects combined

4   Doppler Detection

Target detection or 'lock on' is a post-launch function since many missiles are not in a position to view the target before launch. Those that are able to lock onto a target may break lock due to a launch shock, plume effects, or extremely high feedthrough, which is an unwanted DC component in the spectrum. Thus, the seeker must accomplish target detection at some prescribed time during flight.

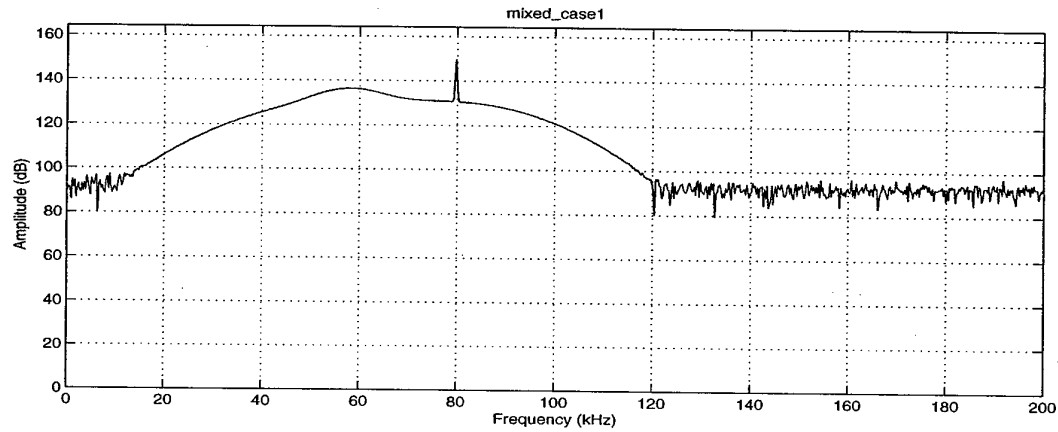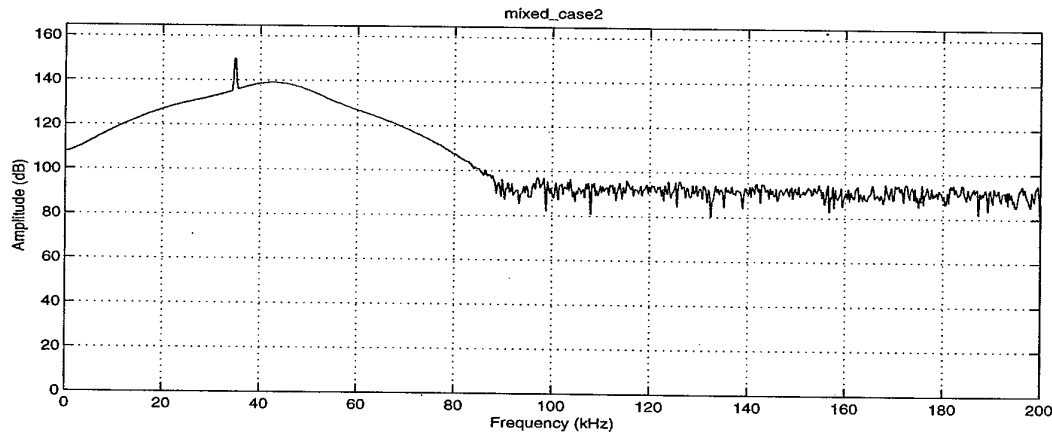Commitment to fire on a target implies that a missile begins its task with the knowledge that a target exists. For a successful firing, the probability of finding a target must be 95 percent or higher. To achieve this, the initial detection threshold is set relatively low, ensuring a high probability of seeing the target. The probability of false alarm is then high, and a suitable detection scheme must be employed to compensate. After a brief summary of detection theory, two different doppler detection schemes are outlined. The first is an optimal scheme for calculating the doppler frequency and amplitude, while the second is a system employed in many semi-active systems. A simulation of the second scheme has been done and the results are summarised in the final section. In a semi-active system, the target's AOA is calculated using monopulse principles, but that is beyond the scope of this report.

4.1   Detection Theory

A target is detected when its amplitude exceeds a threshold value τ. The aim of a good detector is to maximise the probability of detection for a given probability of false alarm. Using the hypothesis and pdf's derived from 3.4.2, we can define the detection and false alarm probabilities for a point X on the spectrum, as:

$$P_d = P(X > \tau | H_1) \quad = \quad \int_\tau^\infty \frac{1}{\sqrt{2\pi\sigma^2}} \exp\left(-\frac{(r-A)^2}{2\sigma^2}\right) dr \tag{36}$$

$$P_{fa} = P(X > \tau | H_0) \quad = \quad \int_\tau^\infty \frac{r}{\sigma^2} \exp\left(-\frac{r^2}{2\sigma^2}\right) dr$$

$$\quad = \quad \exp\left(-\frac{\tau^2}{2\sigma^2}\right), \tag{37}$$

where the variance, σ^2 is the mean noise power and the threshold, τ can be now calculated based on a given false alarm probability,

$$\tau = \sqrt{-2\sigma^2 \ln(P_{fa})}. \tag{38}$$

The case where the noise causes the target's amplitude to be smaller than the threshold is called a miss.

$$P_m = P(X \le \tau | H_1) = \int_{-\infty}^\tau \frac{1}{\sqrt{2\pi\sigma^2}} \exp\left(-\frac{(r-A)^2}{2\sigma^2}\right) dr \tag{39}$$

The following figure shows the regions where each of these definitions are defined.
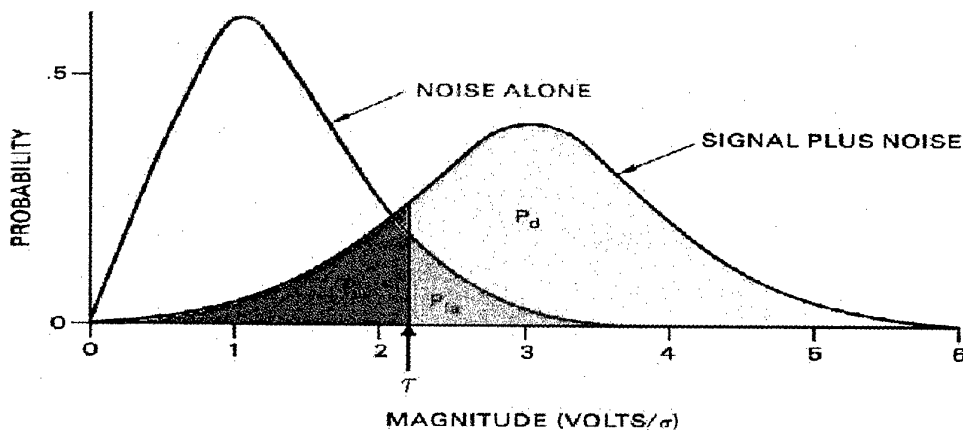
Figure 20: Detection regions

4.2 Optimal Detection

To find an optimal doppler detector, one approach is to maximise a likelihood function containing an accurate model of the signal. This approach has been looked at, but not completed. The derivation is included in Appendix C.

4.3 Non-Optimal Detection

Many different techniques for doppler extraction and tracking have evolved in the last 30 years. The most common systems use combinations of the following three stages: narrow-banding, doppler frequency extraction and doppler tracking.

Narrow-banding

- 'Late narrow-banding' segregates the wanted target signal in doppler frequency from all other signals by a narrow bandpass filter at a late stage in the receiver chain incorporated within the main IF amplifier.

- 'Early narrow-banding' does the segregation as early as possible in the receiver chain, typically before the IF amplifier.

Doppler frequency

- 'Explicit' doppler frequencies are translated to baseband and each doppler frequency is explicitly represented by an AC frequency.

- 'Implicit' doppler frequency remains always as a shift on the carrier frequency and its presence is implied by the change of frequency.

Doppler tracking

- 'Frequency locked loop' - The doppler frequency of the wanted target signal is changed to a second intermediate frequency which is compared with that set by a fixed frequency discriminator. Any maladjustment in frequency is sensed and used to retune the associated LO.

- 'Phase locked loop' - A phase discriminator is used which senses phase difference. This difference is used to retune the LO via an integrator.

Target acquisition is accomplished by sweeping the frequency of the speedgate LO over the designated portion of the doppler bandwidth. The speedgate LO is typically some form of voltage-controlled oscillator (VCO). The linearity of its frequency-voltage characteristic must be carefully controlled to allow precise sweep positioning and a constant sweep rate over the full doppler frequency range of interest. Also, since the VCO forms part of the doppler tracking circuit, control linearity is required to maintain a constant loop gain over its total frequency coverage range. The sweep rate is based on the doppler filter bandwidth and must be slow enough to ensure signal buildup in the filter. The extent of the sweep will differ from system to system, depending on the accuracy of the designation and on operating frequency. Together, the rate and extent of the sweep will determine the number of looks at the target during the available acquisition time and hence the cumulative detection probability.

The actual detection process consists of programming the speedgate LO with a sawtooth of triangular sweep voltage. When the difference between the LO and the target doppler frequencies equals the speedgate filter center frequency, an output is produced at the speedgate discriminator or at a separate amplitude detector. The output signal is then detected and if it exceeds the detection threshold, the search is stopped for a few tens of milliseconds while the signal is examined to verify that it is a coherent target and not a false alarm due to noise. This process of verification examines the signal in the gate for persistence, since a target will remain above the verification threshold while noise will not. Typically, the false alarm rate and the verification time required for each false alarm can be optimised for a given system.

Once the verification threshold has been passed, the speedgate tracking loop is closed and the speedgate is said to be 'locked on'. A valid target is then tracked in frequency using the discriminator, and guidance commands can be extracted from it. A block diagram representing the system is shown in Figure 21, [6].
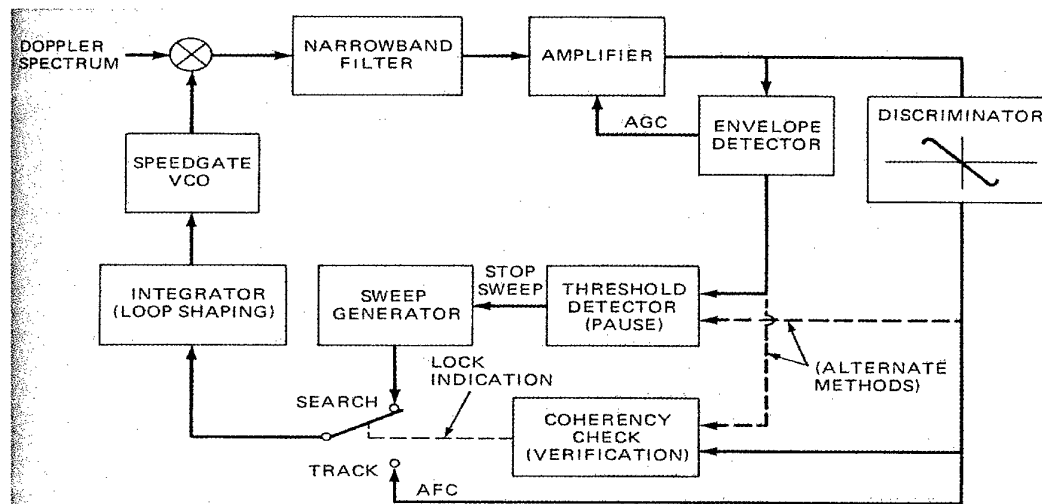
Figure 21: Alternative methods of target detection and verification

4.4 Detection Simulation

A simulation based on Figure 21 was created in MATLAB to test the effect of noise, multipath and sea-clutter on doppler detection. The tracking discriminator is not present in this simulation, since we are only interested in the doppler detection. Consequently, the system is simplified and can be represented by the block diagram in Figure 22.
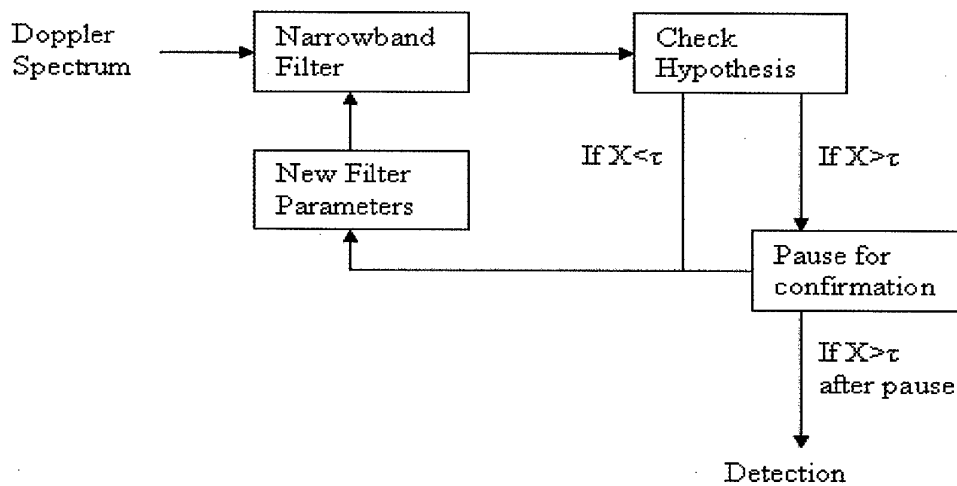
Figure 22: Simplified block diagram for detection and verification

Since the worst case centre frequency of the MLC is at the velocity of the missile, the 'doppler spectrum' or 'passband' can be determined as a portion of the total spectrum coming from the mixer, with the start point set by moving a fixed distance away from the MLC and the end point set at a harmonic of the MLC frequency. In this simulation, the third harmonic was chosen as the end point.

There are a number of important parameters in this simulation. These include the sweep rate or number of steps through the filter bank over a given time, the bandwidth of the filter, whether to overlap the spectrum from one filter block to the next, the detection range, pause length and the detection threshold. The consequence of a non-optimal detection scheme, is that the relationship between the false alarm probability and threshold calculated in section 4.1 no longer holds. The theoretical calculation was based on a system using the entire spectrum and not filtered sections of it. The best analysis that can be done is a comparison of the parameters and how an ideal simulation compares to a realistic one.

4.4.1 Doppler Filter Bank and the Overlapping Spectrum

In Figure 21, a LO is used to mix the doppler spectrum down to baseband, so it can be used in a single filter. For the purposes of modelling the detector, this is simplified by creating a new bandpass finite impulse response filter at each iteration through the detection loop. The overall effect is the same as if a box is drawn around the LO, mixer and filter.

In this simulation, the bandwidth is altered depending on the sweep rate and there is an option for using a 50% overlap between one filter block and the next. This increases the sweep rate and minimises the loss of output when a signal lies between the center frequencies of two filter blocks. For example, if there are N filter blocks in a given time period, then there are $2N - 1$ when using a 50% overlap.
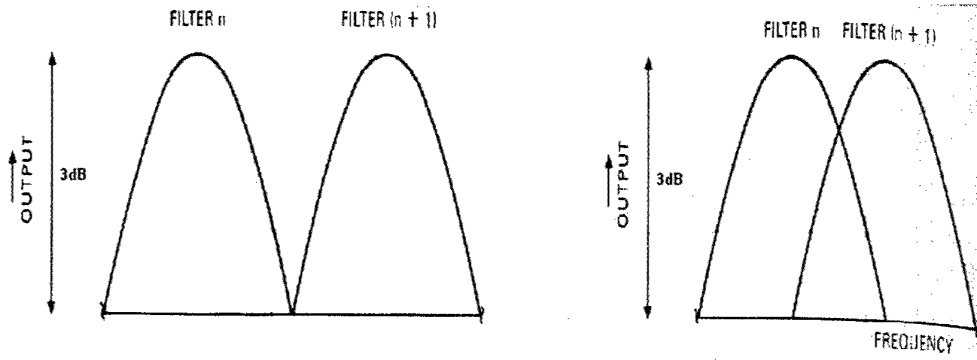

Figure 23: Comparison of non-overlapping and overlapping filters

4.4.2 Detection Range

The detection range is required to test H_1, the case where there is a signal and noise present. It defines the bounds where a correct detection takes place relative to the center frequency. If a detection takes place outside the detection range, it is deemed a miss.
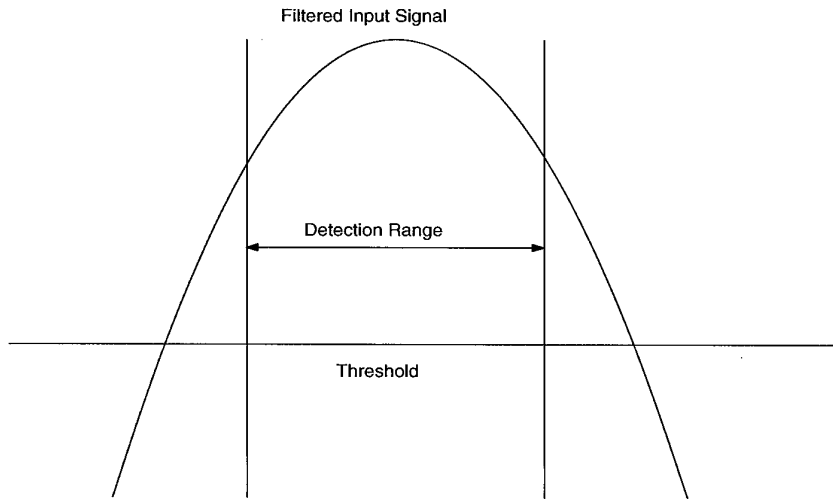
Filtered Input Signal

Detection Range

Threshold

Figure 24: Detection range

4.4.3 Pause Length

The pause length determines how long the system waits before deciding if a signal contains a target and not noise. If the pause length is longer, there will be less noise that can be mistaken for a target, but the miss rate will be higher since there is a longer time interval where a target can not be detected. The following figure has a target with noise present for the first 15 time periods, then noise only for 15 time periods. There are four pairs of images, each pair having the thresholded only scenario on the left and the thresholded and delayed scenario on the right. If a filter block is white, then it has exceeded the threshold and is a detection.

The target is clear in each of the scenarios as the constant line in the bottom left. As the pause length increases, more noise is removed until only the target is seen in the final scenario on the bottom right image.

4.5 Receiver Operating Characteristics

To do a complete comparison of the different parameters, a common technique is to vary the threshold, and measure the false alarm and detection rates. This is called a Receiver Operating Characteristic (ROC). Recall the two hypothesis:

$$H_0 : \quad \text{noise only is present}$$
$$H_1 : \quad \text{signal and noise are present}$$

The axes of the ROC curve relate H_0 to the false alarm rate and H_1 to the detection rate using the definitions from section 4.1.

The following table describes the default variables used in the simulation for all parameters except the one being varied.
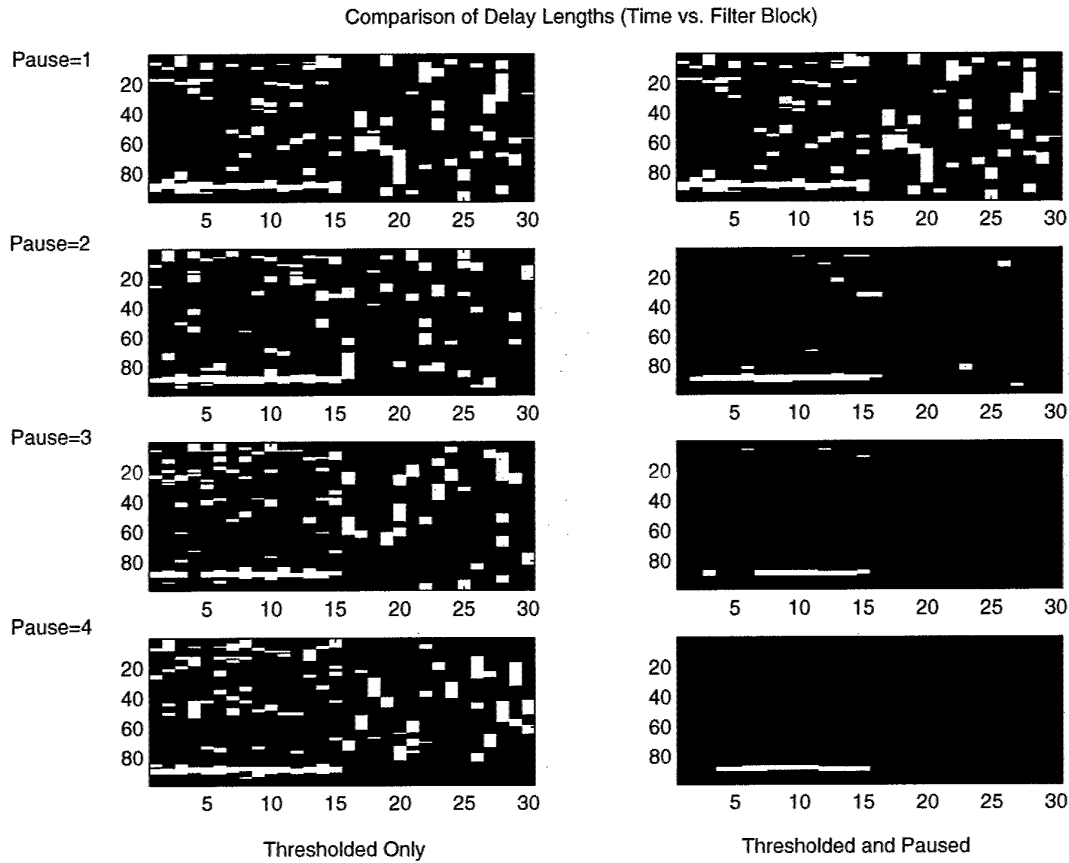
Figure 25: Comparison of pause lengths on detection

Table 2: Detection parameters

50% Overlap	Threshold Pause (time periods)	Detection Range	Sweep Rate
No	2	3kHz	50

The following ROC curves were then obtained by running both scenarios 75 times for H_0 and 75 times for H_1. The sea-clutter and multipath effects were included in the simulation, while the receiver noise was re-simulated each time to generate the randomness required.

The effect of overlapping filter banks caused an increase in the false alarm rate for both scenarios. This is a consequence of the increased sweep rate required to compensate for the overlapping filter bank. The second scenario has approximately twice the false alarm rate than the first due to the closer proximity of the sea-clutter peak. Further work could be done to verify this by changing the position of the sea-clutter and observing the simulation results.
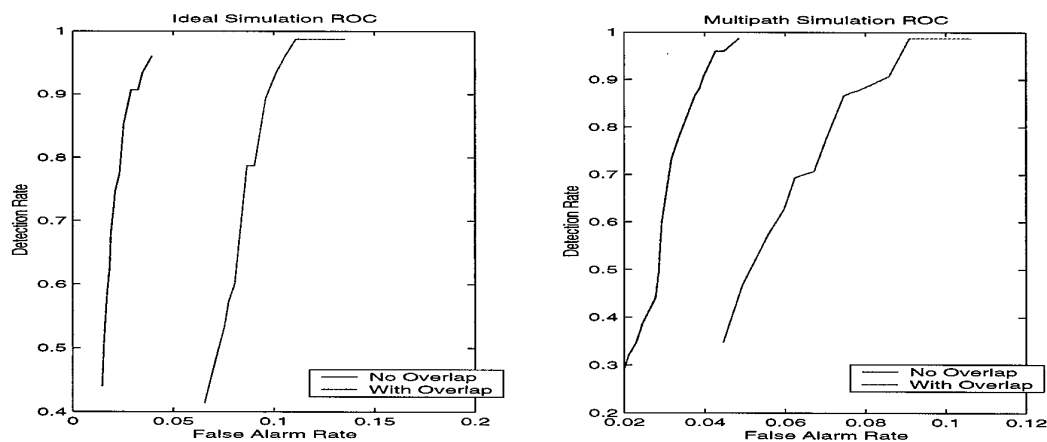
Figure 26: ROC curve for varying overlap - scenario 1
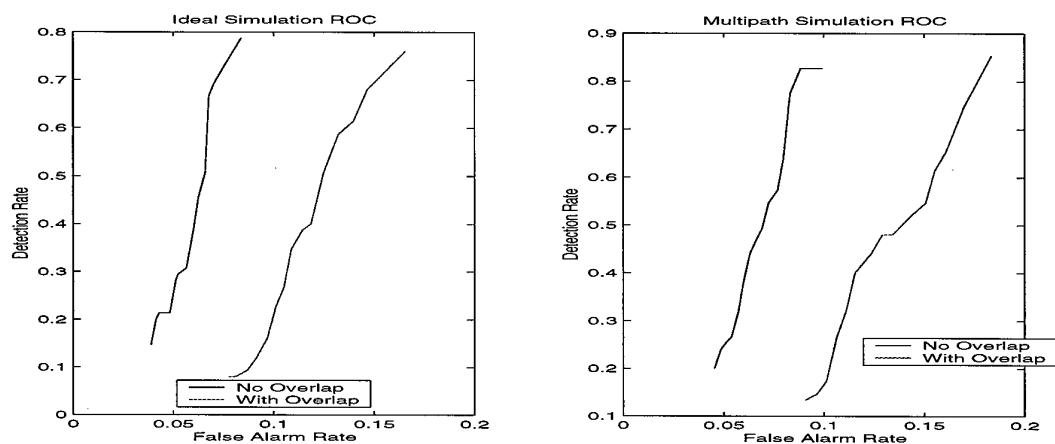
Figure 27: ROC curve for varying overlap - scenario 2

The curves look very similar in both scenarios, though the second one has a slightly higher false alarm rate. There does not appear to be many differences between the ideal and the multipath cases indicating that this variable is independent of the scenario. Clearly though, as the pause length increases, the false alarm rate decreases in each case.
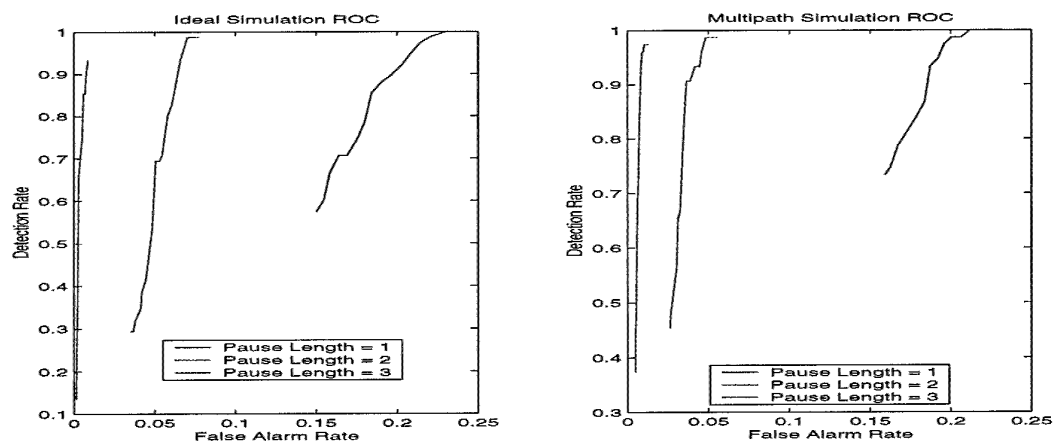
Figure 28: ROC curve for varying threshold pause - scenario 1
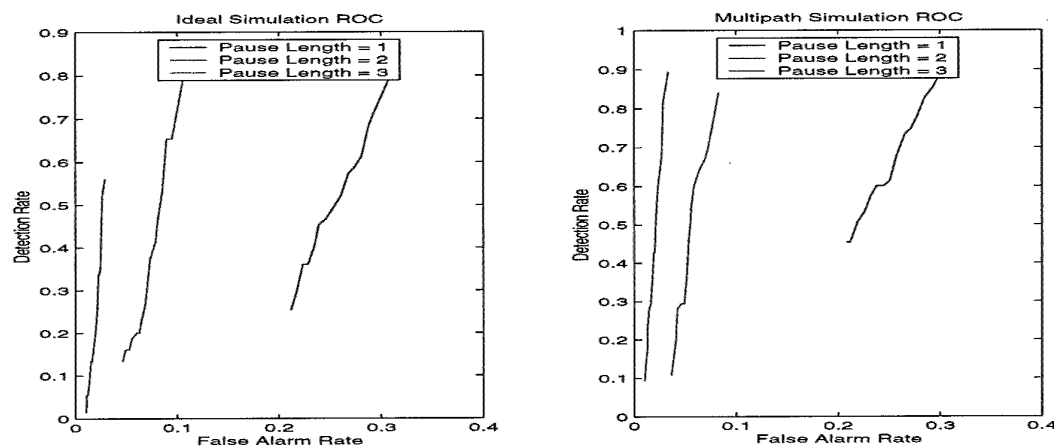
Figure 29: ROC curve for varying threshold pause - scenario 2

There are many interesting conclusions that can be drawn from these results. Firstly, when there is a small detection range, the multipath case performs better due to its larger frequency spread. However, in the second scenario, the 1kHz detection range proved to be too narrow to pass the detection threshold. The trend is that larger detection ranges give lower false alarm rates until a limit is reached and then they have an adverse affect in the multipath case of Figure 30.
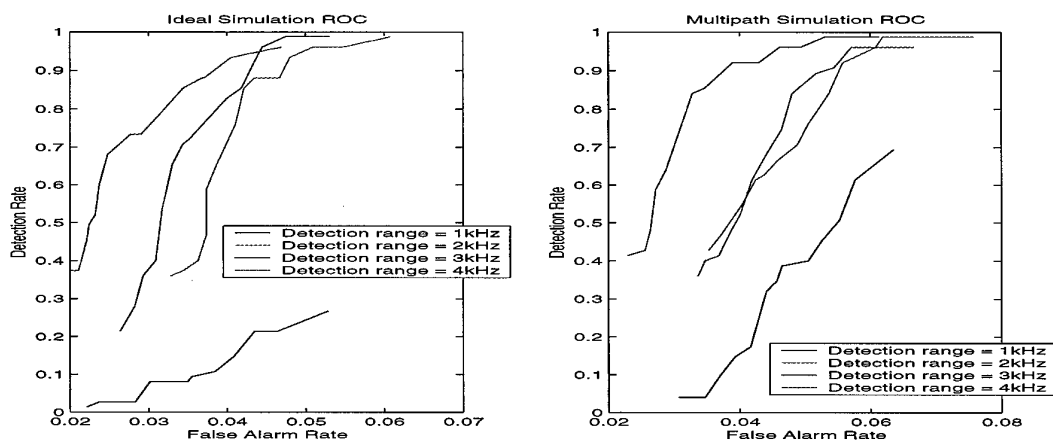
Figure 30: ROC curve for varying detection range - scenario 1
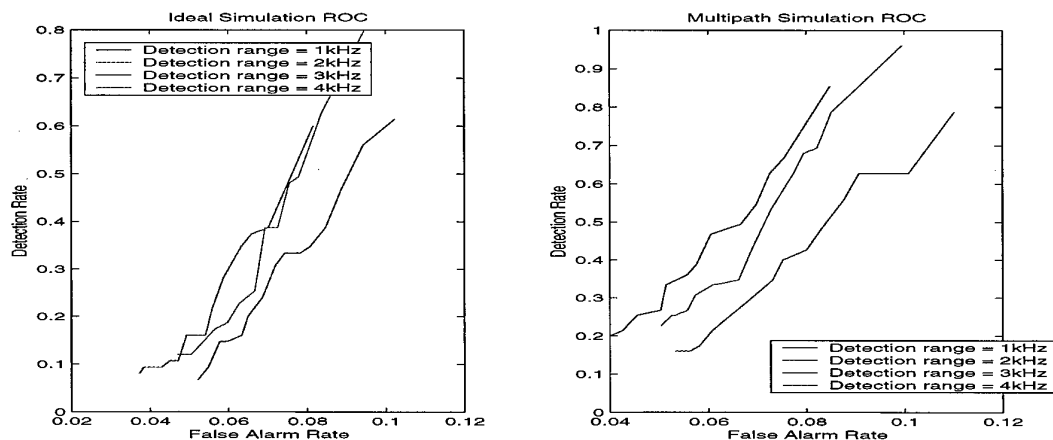
Figure 31: ROC curve for varying detection range - scenario 2

All but the multipath case in scenario 1 were able to give distinctive results, as the curves overlap. The trend is as the sweep time increases, the false alarm rate gets higher. This is due to the bandpass filter having a smaller bandwidth as the sweep time increases. There is also a slight increase in false alarm rate for scenario 2. From these results there are a few conclusions that can be drawn:

- The multipath case did not give significantly worse results, as the broad sea-clutter overlapped the multipath component.

- Using a 50% overlap in the filter bank gives a higher false alarm rate.

- A longer threshold pause gives a lower false alarm rate and is independent of the scenario.

- The trend for the detection range shows that larger detection ranges give lower false alarm rates until an upper limit is reached.

- A greater sweep time (filter bank) gives a higher false alarm rate.
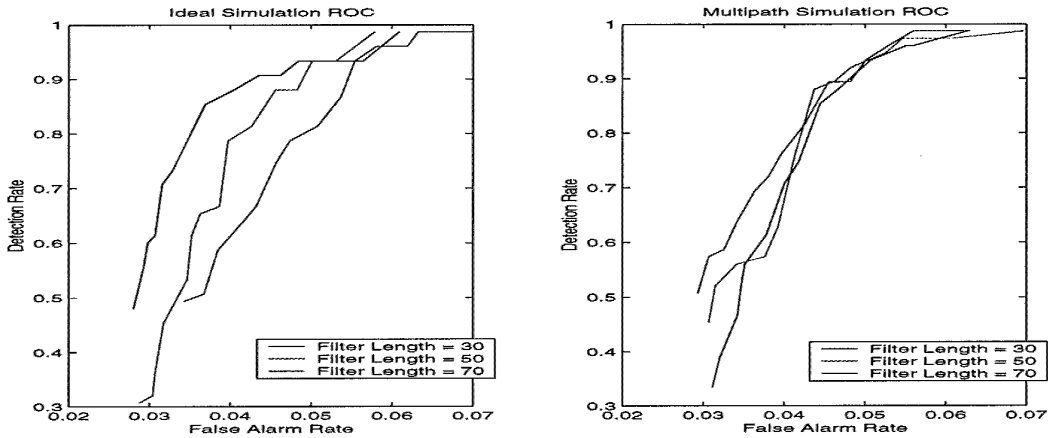
Figure 32: *ROC curve for varying sweep rates - scenario 1*
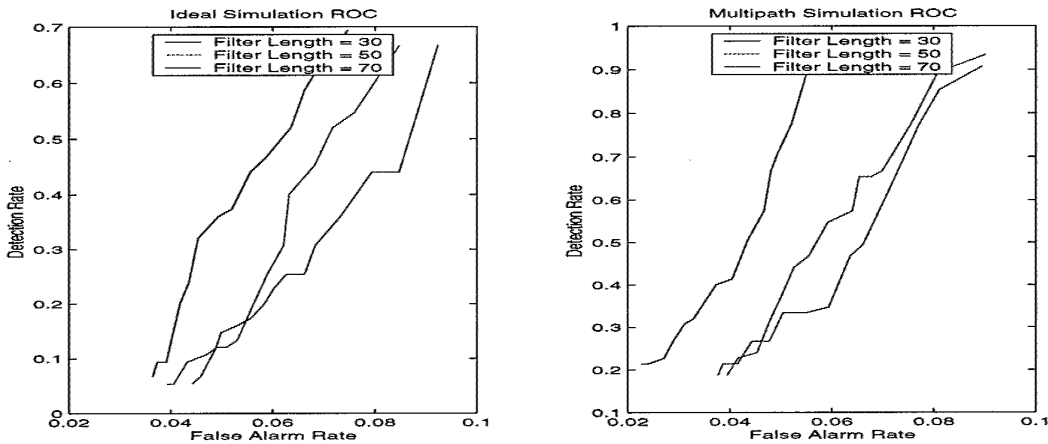
Figure 33: *ROC curve for varying sweep rates - scenario 2*

5   Conclusions and Future Work

The Simulink simulation worked well and demonstrated the effects of multipath, sea-clutter and receiver noise on an ideal simulation. It is clear that mixing the multipath and sea-clutter caused the spectrum to spread widely and this in turn gave some interesting detection results. There are a number of improvements that could build on this section:

- Multipath with a reduced amplitude could be added to the front signal.

- A small randomness in the frequency offset for the multipath signal could be used to more accurately model real life. This would add extra frequency components during the convolution.

- A comparison on different amounts of frequency spread could be included.

- The models for multipath and sea-clutter could be improved to more accurately model different sea states and other atmospheric conditions.

The optimal detection scheme needs some more work to provide an alternative means to determine the doppler frequency and amplitude of the filtered spectrum. The non-optimal detection scheme gave good results and led to a number of observations. These are repeated for completeness:

- The multipath case did not give significantly worse results, as the broad sea-clutter overlapped the multipath component.

- Using a 50% overlap in the filter bank gives a higher false alarm rate.

- A longer threshold pause gives a lower false alarm rate and is independent of the scenario.

- The trend for the detection range shows that larger detection ranges give lower false alarm rates until an upper limit is reached. More extensive simulations of this variable could give more conclusive results and be used to optimise the detection range for this system.

- A greater sweep time gives a higher false alarm rate, due to the decreasing bandwidth of the bandpass filter. Again, further simulations could be used to find an optimal sweep time for this system.

The detection simulation could be improved by increasing the length of time that each hypothesis was tested over and increasing the number of points on the ROC curves. Further simulations could also be used to optimise the detection range and the sweep time for this system. There are also a few alternative detection schemes that could be used to compare with this one, such as the 'n out of m detector', [6], detectors based on a 'constant false alarm rate' and schemes which incorporate both detection and tracking.

Finally, putting the seeker in the real world would involve the target moving in different directions and at different velocities. The seeker would need to compensate by changing its trajectory and velocity. Both of these changes would vary the doppler measured at the front receiver. In the future, this model could be introduced into a larger system where there are moving targets and existing sea-clutter and multipath models. Testing the effect under these dynamic conditions is a much larger project, but could easily extend this work. The ultimate outcome would then be to verify 'Hardware In the Loop' simulations with the measured output doppler and AOA.

References

1. W.V.Andrew, *The effects of Multi-path Propogation on Low-Altitude Detect Pulsed-Doppler RADAR Systems*, December 1990, Arizona State University.

2. W.Lippincott, *Sea Surface Multipath Effects on Ship Radar Radiated Power Determination*, Advanced Systems Technology Branch, Space Systems Development Department.

3. R.M.Smith, J.Y.Yee, C.S. An and A.L.Haun *Simulation of Multipath for Semi-active Missiles*, AGARD CP-473, Turkey 1990.

4. D.Lewis *Principles of Naval Architecture*, 1983, Society of Naval Architects and Marine Engineers, August 1997.

5. C. Beard and I.Katz *The Dependence of Microwave Radio Spectra on Ocean Roughness and Wave Spectra*, Transactions on Antennas and Propagation, 1957

6. M.Skolnik, *'RADAR Handbook - Second Edition*, 1990, McGraw-Hill Inc.

7. D.A.James, *'Radar Homing Guidance for Tactical Missiles*, 1986, Royal Military College of Science Shrivenham.

8. G.W.Stimson, *Introduction to Airborne RADAR*, 1983, Hughes Aircraft Co., El Segundo, CA.

9. R.Smith, *Multipath Math Model and Implementation Guide - Revision No. 1*, July 29, 1986, Missile Software Branch, China Lake, California USA.

10. B.Moran *Detection, Estimation and Classification*, MSIP Lecture notes, March 2000.

11. B.Mahafza *Radar Systems Analysis and Design Using MATLAB*, Chapman and Hall/CRC, 2000

Appendix A   Ideal Simulation Verification

The Simulink model used for the simulation is shown in Figure A1. The low pass filter is implemented in Simulink by first creating it in MATLAB, then passing its frequency response to be multiplied in the frequency domain.
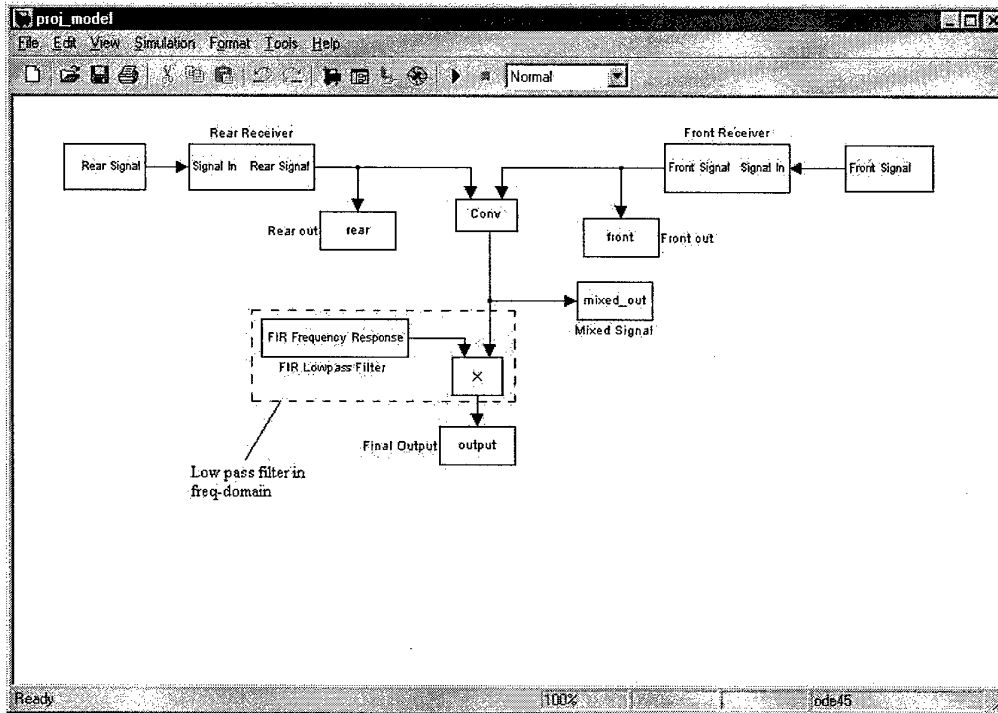
Figure A1: Simulink model

Using this model, scenario 1 was run with a rear doppler of -30kHz and a front doppler of 50kHz. With the carrier reference set to 1MHz rather than 10GHz for the convenience of demonstration, the frequency of the front signal should be 1MHz+50kHz=1.05MHz and the frequency for the rear signal should be 1MHz-30kHz=0.97MHz. The front and rear signals are shown in Figure A2:
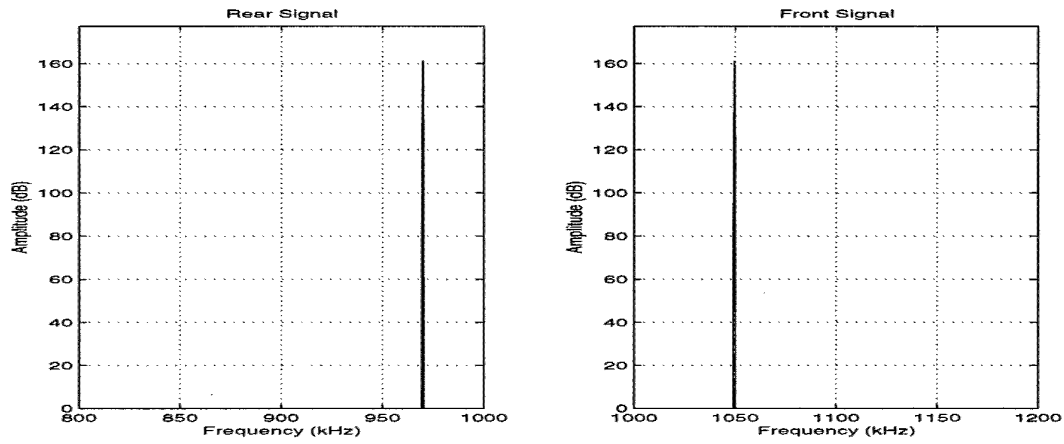
Figure A2: Front and rear signals

It is clear that the signals are at the correct frequencies, and hence the convolution places the final doppler at the difference of the front and rear frequencies, which is 80kHz. Figure 6 has been reproduced to show this.
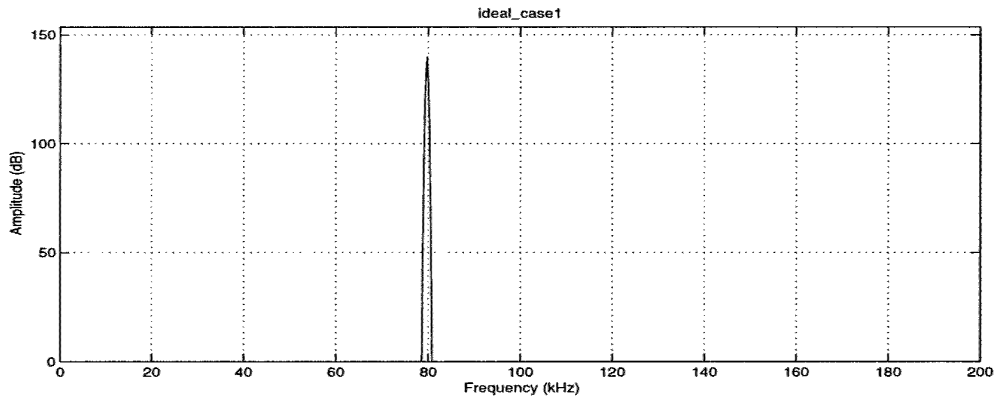
Figure A3: Ideal scenario 1 repeated

Appendix B Sea-clutter Frequency Calculation

To calculate the sea-clutter center frequency shift, a Gaussian shaped spectrum is approximated by the Fourier Transform of a cosine function, where the mean is approximated by the frequency of the cosine. The exact frequency was then determined by the following signal definitions in the time domain:

$$S_F(t) = \sin(2\pi(f_c + f_F)t)$$
$$S_R(t) = \sin(2\pi(f_c + f_R)t)$$
$$S_C(t) = \sin(2\pi(f_c + f_{cl})t)$$

where the new front signal is now represented as in equation 19 and the mixing is a multiplication, since the signals are represented in the time domain. The final spectrum becomes:

$$
\begin{aligned}
S_D(t) &= S_R(t)[S_F(t) + S_C(t)] \\
&= \frac{1}{2}\cos(2\pi(f_F - f_R)t) + \frac{1}{2}\cos(2\pi(f_{cl} - f_R)t) + \\
&\quad \frac{1}{2}\cos(2\pi(2f_c + f_R + f_F)t) + \frac{1}{2}\cos(2\pi(2f_c + f_R + f_{cl})t) \quad \text{(B1)}
\end{aligned}
$$

where the desired sea-clutter frequency is now shifted by the rear doppler frequency.

Appendix C   Optimal Detection

¿From the complete simulation in section 3.5, we can define a signal $s(f)$, in the frequency domain with all three effects added, sea-clutter, multipath and noise. Mathematically, $s(f)$ is multiplied by a Gaussian with unknown amplitude a_T, mean f_T and known variance σ_T^2 and contains additive zero mean white noise, $n(f)$ with variance σ^2:

$$s(f) = a_T \exp\left(-\frac{(f - f_T)^2}{2\pi\sigma_T^2}\right) + n(f) \tag{C1}$$

The probability density of $s(f)$ is given by

$$P_{a_T;f_T}(s) = \frac{1}{(\sqrt{2\pi\sigma^2})^N} \exp\left(-\frac{1}{2\pi\sigma^2} \sum_f \left| s(f) - a_T \exp\left(-\frac{(f - f_T)^2}{2\sigma_T^2}\right)\right|^2\right) \tag{C2}$$

and the likelihood function is obtained by taking the log of the probability density:

$$L_s(a_T; f_T) = -\frac{1}{2\pi\sigma^2} \sum_f \left| s(f) - a_T \exp\left(-\frac{(f - f_T)^2}{2\sigma_T^2}\right)\right|^2 \tag{C3}$$

If we differentiate this with respect to the two unknowns, a_T and f_T, we get:

$$\frac{\partial L_s}{\partial a_T} = \frac{1}{\pi\sigma^2} \sum_f \left[s(f) - a_T \exp\left(-\frac{(f - f_T)^2}{2\sigma_T^2}\right)\right] \exp\left(-\frac{(f - f_T)^2}{2\sigma_T^2}\right) \tag{C4}$$

$$\frac{\partial L_s}{\partial f_T} = \frac{2}{\pi\sigma^2} \sum_f \left[s(f) - a_T \exp\left(-\frac{(f - f_T)^2}{2\sigma_T^2}\right)\right] a_T \exp\left(-\frac{(f - f_T)^2}{2\sigma_T^2}\right) \frac{(f - f_T)}{2\sigma_T^2} \tag{C5}$$

If these two equations are then equated to zero, they become

$$\sum_f \left[s(f) - a_T \exp\left(-\frac{(f - f_T)^2}{2\sigma_T^2}\right)\right] \exp\left(-\frac{(f - f_T)^2}{2\sigma_T^2}\right) = 0 \tag{C6}$$

$$\sum_f \left[s(f) - a_T \exp\left(-\frac{(f - f_T)^2}{2\sigma_T^2}\right)\right] \exp\left(-\frac{(f - f_T)^2}{2\sigma_T^2}\right) (f - f_T) = 0 \tag{C7}$$

Equation C6 can then be rearranged

$$\sum_f s(f) \exp\left(-\frac{(f - f_T)^2}{2\sigma_T^2}\right) = a_T \sum_f \exp\left(-\frac{(f - f_T)^2}{2\sigma_T^2}\right) \tag{C8}$$

to show that the RHS represents a Gaussian probability density function, with mean f_T and variance σ_T^2.

$$\sum_f \frac{1}{\sqrt{2\pi\sigma_T^2}} \exp\left(-\frac{(f - f_T)^2}{2\sigma_T^2}\right) = 1 \tag{C9}$$

Hence, equation C8 becomes

$$\sum_f s(f) \exp\left(-\frac{(f - f_T)^2}{2\sigma_T^2}\right) = a_T \sqrt{2\pi\sigma_T^2} \tag{C10}$$

and can be rearranged to give an expression for a_T.

$$a_T = \frac{1}{\sqrt{2\pi\sigma_T^2}} \sum_f s(f) \exp\left(-\frac{(f-f_T)^2}{2\sigma_T^2}\right) \tag{C11}$$

Now, if equation C7 is rearranged in a similar way,

$$\sum_f s(f)(f-f_T) \exp\left(-\frac{(f-f_T)^2}{2\sigma_T^2}\right) = a_T \sum_f \exp\left(-\frac{(f-f_T)^2}{2\sigma_T^2}\right)(f-f_T) \tag{C12}$$

and we use the fact that $E(f-f_T) = 0$. Then,

$$\sum_f \exp\left(-\frac{(f-f_T)^2}{2\sigma_T^2}\right)(f-f_T) = 0 \tag{C13}$$

and equation C12 becomes

$$\sum_f s(f)(f-f_T) \exp\left(-\frac{(f-f_T)^2}{2\sigma_T^2}\right) = 0. \tag{C14}$$

The next step is to define

$$g(f-f_T) = \exp\left(-\frac{(f-f_T)^2}{2\sigma_T^2}\right) \quad .$$

and notice that equation C14 is the same as

$$\sum_f s(f)g'(f-f_T) \sim \int_f s(f)g'(f-f_T)df = 0 \tag{C15}$$

Using integration by parts, this becomes

$$s(f)g(f-f_T)\Big|_f - \int_f s'(f)g(f-f_T)df = 0 \tag{C16}$$

where the first part tends to 0. Thus

$$\int_f s'(f)g(f-f_T)df = 0 \tag{C17}$$

Now, using Parsevals Identity:

$$\int \mathcal{F}\{F(f)\}\mathcal{F}\{G(f)\}df = \frac{1}{2\pi} \int f(t)g(t)dt \tag{C18}$$

we can take the Fourier Transform of this expression, where

$$\mathcal{F}\{s'(f)\} = ts(t) \tag{C19}$$
$$\mathcal{F}\{g(f-f_T)\} = e^{-2\pi i f_T t}\mathcal{F}\{g(f)\}$$
$$= e^{-2\pi i f_T t}C \exp\left[-\frac{\sigma^2 t^2}{2}\right]. \tag{C20}$$

Thus, equation C17 becomes

$$\int ts(t) \exp\left[-\frac{\sigma^2 t^2}{2}\right] e^{-2\pi f_T t}dt = 0 \tag{C21}$$

At this stage, a numerical solution in MATLAB is required to solve this equation. Work on this method is still in progress.

Appendix D   Range Equation

Here is the range equation for a bi-static radar, as used in the semi-active case in this report.

$$(R_1^2 R_2^2)_{max} = \frac{P_I \sigma G_I A_m}{(4\pi)^2 L S_{min}} \qquad (D1)$$

where,

R_1 = range illuminator-target (m)

R_2 = range target-missile (m)

P_I = illuminator power (W)

σ = radar cross section (m^2)

G_I = illuminator gain (dB)

A_m = effective aperture of the receiving antenna (m^2)

L = loss factor for miscellaneous losses (dB)

and, $S_{min} = F_n(kT_o B)(S:N)_{min}$, where

$(S:N)_{min}$ = minimum detectable signal level at the receiver output (dB)

F_n = receiver noise figure

B = receiver bandwidth (Hz)

k = Boltzmann's constant 1.38 x $10^{-23}(Ws/^0K)$

T_0 = absolute temperature of the resistor representing the external noise (^0K)

DISTRIBUTION LIST

Signal Processing in a Semi-active Seeker

Luke Rosenberg, Yiding Hu and Bill Moran

	Number of Copies
DEFENCE ORGANISATION	
Task Sponsor	
Director General Air Development	1
S&T Program	
Chief Defence Scientist	
FAS Science Policy	
AS Science Corporate Management	1
Director General Science Policy Development	
Counsellor, Defence Science, London	Doc Data Sheet
Counsellor, Defence Science, Washington	Doc Data Sheet
Scientific Adviser to MRDC, Thailand	Doc Data Sheet
Scientific Adviser Joint	1
Navy Scientific Adviser	Doc Data Sheet
Scientific Adviser, Army	Doc Data Sheet
Air Force Scientific Adviser	Doc Data Sheet
Scientific Adviser to the DMO M&A	Doc Data Sheet
Scientific Adviser to the DMO ELL	Doc Data Sheet
Information Sciences Laboratory	
Bill Moran	1
Systems Sciences Laboratory	
Chief, WSD	Doc Data Sheet
RLAWS WSD	1
RLMWS WSD	1
HMS WSD	1
HRFS WSD	1
HWSA WSD	1
Luke Rosenberg	1
Yiding Hu	1
Ninh Duong	1
Peter Simms	1
Richardo Nazar	1
DSTO Library and Archives	
Library, Fishermans Bend	Doc Data Sheet

Library, Edinburgh	1
Library, Sydney	Doc Data Sheet
Library, Stirling	Doc Data Sheet
Library, Canberra	Doc Data Sheet
Australian Archives	1

Capability Systems Division

Director General Maritime Development	Doc Data Sheet
Director General Land Development	1
Director General Information Capability Development	Doc Data Sheet

Office of the Chief Information Officer

Deputy Chief Information Officer	Doc Data Sheet
Director General Information Policy and Plans	Doc Data Sheet
AS Information Strategies and Futures	Doc Data Sheet
AS Information Architecture and Management	Doc Data Sheet
Director General Australian Defence Simulation Office	Doc Data Sheet

Strategy Group

Director General Military Strategy	Doc Data Sheet
Director General Preparedness	Doc Data Sheet

Navy

SO (SCIENCE), COMAUSNAVSURFGRP, NSW	Doc Data Sheet
Director General Navy Capability, Performance and Plans, Navy Headquarters	Doc Data Sheet
Director General Navy Strategic Policy and Futures, Navy Headquarters	Doc Data Sheet

Army

ABCA National Standardisation Officer, Land Warfare Development Sector, Puckapunyal	Doc Data Sheet
SO (Science), Deployable Joint Force Headquarters (DJFHQ)(L), Enoggera QLD	Doc Data Sheet
SO (Science), Land Headquarters (LHQ), Victoria Barracks, NSW	Doc Data Sheet

Air Force

Intelligence Program

DGSTA, Defence Intelligence Organisation	1
Manager, Information Centre, Defence Intelligence Organisation	1
Assistant Secretary Corporate, Defence Imagery and Geospatial Organisation	Doc Data Sheet

Defence Materiel Organisation

Deputy CEO	Doc Data Sheet
Head Aerospace Systems Division	Doc Data Sheet
Head Maritime Systems Division	Doc Data Sheet
Chief Joint Logistics Command	Doc Data Sheet
Head Materiel Finance	Doc Data Sheet

Defence Libraries

Library Manager, DLS-Canberra	Doc Data Sheet
Library Manager, DLS-Sydney West	Doc Data Sheet

UNIVERSITIES AND COLLEGES

Australian Defence Force Academy Library	1
Head of Aerospace and Mechanical Engineering, ADFA	1
Deakin University Library, Serials Section (M List), Geelong, Vic	1
Hargrave Library, Monash University	Doc Data Sheet
Librarian, Flinders University	1

OTHER ORGANISATIONS

National Library of Australia	1
NASA (Canberra)	1
Government Publications Librarian, State Library of New South Wales	1

INTERNATIONAL DEFENCE INFORMATION CENTRES

US Defense Technical Information Center	2
UK Defence Research Information Centre	2
Canada Defence Scientific Information Service	1
NZ Defence Information Centre	1

ABSTRACTING AND INFORMATION ORGANISATIONS

Library, Chemical Abstracts Reference Service	1
Engineering Societies Library, US	1
Materials Information, Cambridge Scientific Abstracts, US	1
Documents Librarian, The Center for Research Libraries, US	1

INFORMATION EXCHANGE AGREEMENT PARTNERS

National Aerospace Laboratory, Japan	1
National Aerospace Laboratory, Netherlands	1

SPARES

Total number of copies: 43

DEFENCE SCIENCE AND TECHNOLOGY ORGANISATION DOCUMENT CONTROL DATA		1. CAVEAT/PRIVACY MARKING

2. TITLE	3. SECURITY CLASSIFICATION		
Signal Processing in a Semi-active Seeker	Document (U) Title (U) Abstract (U)		

4. AUTHORS	5. CORPORATE AUTHOR
Luke Rosenberg, Yiding Hu and Bill Moran	Systems Sciences Laboratory PO Box 1500 Edinburgh, South Australia, Australia 5111

6a. DSTO NUMBER	6b. AR NUMBER	6c. TYPE OF REPORT	7. DOCUMENT DATE
DSTO–TR–1606	013-164	Technical Report	August, 2004

8. FILE NUMBER	9. TASK NUMBER	10. SPONSOR	11. No OF PAGES	12. No OF REFS
	AIR 99/133	DGAD	38	11

13. DOWNGRADING / DELIMITING INSTRUCTIONS	14. RELEASE AUTHORITY
Not Applicable	Chief, Weapons Systems Division

15. SECONDARY RELEASE STATEMENT OF THIS DOCUMENT

This work was undertaken as part of a Masters degree in conjunction with the Cooperative Research Centre for Sensor Signal and Information Processing (CSSIP).

OVERSEAS ENQUIRIES OUTSIDE STATED LIMITATIONS SHOULD BE REFERRED THROUGH DOCUMENT EXCHANGE, PO BOX 1500, EDINBURGH, SOUTH AUSTRALIA 5111

16. DELIBERATE ANNOUNCEMENT

Approved for Public Release

17. CITATION IN OTHER DOCUMENTS

No Limitations

18. DEFTEST DESCRIPTORS

19. ABSTRACT

In publicly available generic digital simulations of semi-active Radio Frequency (RF) seekers, the combined effect of multipath, sea-clutter and other non-linear noise sources are mainly studied in individual models, while the effect in the seekers data processing has not been systematically investigated. This report details these effects and how they have been combined to model the signal processing blocks inside a semi-active seeker. A basic doppler detection scheme is then simulated to investigate the consequence of these effects on target detection.

Australian Government

Department of Defence

Defence Science and
Technology Organisation